haematologica
Journal of the Ferrata Storti Foundation

Divergent processing of FVIII light chain variants: secretory potential *versus* proteasomal retention

by Heike Singer, Payal Chawla, Katrin J. Czogalla-Nitsche, Pujan Engels, Francesco Forin, Marc Sylvester, Melanie Rath, Jens Müller, Tobias Feist, Behnaz Pezeshkpoor, Rawya Al-Rifai, Osman El-Maarri and Johannes Oldenburg

Received: May 15, 2025.
Accepted: November 14, 2025.

Citation: Heike Singer, Payal Chawla, Katrin J. Czogalla-Nitsche, Pujan Engels, Francesco Forin, Marc Sylvester, Melanie Rath, Jens Müller, Tobias Feist, Behnaz Pezeshkpoor, Rawya Al-Rifai, Osman El-Maarri and Johannes Oldenburg. Divergent processing of FVIII light chain variants: secretory potential versus proteasomal retention.
Haematologica. 2025 Nov 27. doi: 10.3324/haematol.2025.288250 [Epub ahead of print]

Divergent processing of FVIII light chain variants: secretory potential versus proteasomal retention

Heike Singer,[1,*] Payal Chawla,[1,*] Katrin J. Czogalla-Nitsche,[1] Pujan Engels,[1] Francesco Forin,[1] Marc Sylvester,[2] Melanie Rath,[1] Jens Müller,[1] Tobias Feist,[1] Behnaz Pezeshkpoor,[1] Rawya Al-Rifai,[1] Osman El-Maarri,[1] Johannes Oldenburg,[1,#]

[1]Institute of Experimental Haematology and Transfusion Medicine, University of Bonn, Germany

[2]Medical Faculty, Core Facility Mass Spectrometry, Institute of Biochemistry and Molecular Biology, University of Bonn, Bonn, Germany

[*]HS and PC contributed equally as co-first authors

#Correspondence: johannes.oldenburg@ukbonn.de

RESOURCE AVAILABILITY

Lead contact

Further information and requests for resources and reagents should be directed to and will be fulfilled by the lead contact, Prof. Dr. med. Johannes Oldenburg (johannes.oldenburg@ukbonn.de).

Resource availability

Further information and requests for resources and reagents should be directed to and will be fulfilled by the lead contact upon request.

Data and code availability

Original western blot images and microscopy data reported in this paper will be shared by the lead contact upon request. Any additional information required to reanalyze the data reported in this paper is available from the lead contact upon request.

DECLARATION OF INTERESTS

The authors declare no competing interests.

SUPPLEMENTAL INFORMATION

Document S1. Figures S1–S14 and Table S1-S4

FUNDING

This work was supported, in part, by funding from Bayer Vital #KEL056 (to JO/OEM/HS), ECIA 2017 from Bayer (to HS), Horizon 2020 Marie Curie ITN EDUC8 grant #859974 (to PC), DFG Emmy Noether Programme #CZ-245 (to KJCN) and a scientific grant from Octapharma #OCT-23-002 (to JO/HS).

ACKNOWLEDGEMENTS
Primary LSECs were a kind gift from Dr. Osman El-Maarri. FVIII reference peptide library was created using a plasma derived FVIII product and the experiment was conducted by Dr. Samhitha Urs and Dr. Arijit Biswas. Protein identification was performed at the Core Facility Analytical Proteomics, Institute of Biochemistry and Molecular Biology, Medical Faculty, University of Bonn Funded by the Deutsche Forschungsgemeinschaft (DFG, German Research Foundation) – Project number 386936527. We also thank the Bonn Haemophilia Centre, in particular Dr. C. Klein and Dr. K. Herbst, for their support in collecting patient blood samples.

AUTHOR CONTRIBUTIONS
Conceptualization, H.S. and J.O.; development of $F8^{-/-}$ KO, F.F., K.J.C., H.S.; establishment of vEC H.S., R.A.; establishment of iLEC and iLSEC, H.S., P.C.; analysis and interpretation of data cell culture, RT-qPCR, western blot H.S., P.C., T.F.; analysis and interpretation of data MassSpec; P.C., M.S., H.S.; analysis and interpretation of data cytokine influence, H.S., P.E; FACS, P.C., J.M.; technical support, M.R.; HLA genotyping, B.P.; in silico peptide binding prediction, H.S., P.C.; writing original draft, H.S. and P.C.; writing, review & editing., P.C., O.E.M, B.P.; supervision, H.S., J.O.

ABSTRACT

In 20-30% of severe Haemophilia A (HA) patients, FVIII replacement therapy is hindered by inhibitory antibodies. Nonsense mutations in the FVIII light chain (A3-C1-C2) carry a higher risk of inhibitor formation than those in the heavy chain (A1-A2-B). The underlying molecular mechanism remains unclear. Using induced pluripotent stem (iPS) cells from HA patients, we developed two types of endothelial cell models (iLEC and iLSEC) that mimic native *F8* mRNA expression and protein synthesis. Immunoassays detected FVIII protein in wild-type, I22I, and two high inhibitor risk light chain variants (R1960X, R2228X). Co-staining with ER markers (PDI, BiP) revealed differential processing: R1960X exhibit enhanced proteasomal degradation with SEL1L, essential for MHC-I peptide loading, possibly contributing to higher immunogenicity. In contrast, R2228X showed a pattern more similar to wild type, suggesting partial secretory potential. Although a mild co-localization with SEL1L was observed, it was not significant. Clinically, this patient did not develop inhibitors. In addition, exploratory *in silico* peptide binding predictions suggested that R1960X may generate a higher number of FVIII-derived epitopes presented via patient-specific HLA alleles compared to R2228X, further supporting differential immunogenicity. The intron 22 inversion variant also showed detectable FVIII protein, which was deglycosylated and retained in the ER but did not co-localize with SEL1L; no inhibitor was observed in this case either. This cellular model shows reduced variability compared to primary cells, enabling patient specific FVIII variant analyses, including intracellular processing, within the genetic background of the respective patient.

INTRODUCTION

Haemophilia A (HA) is an X-linked disorder resulting from mutations in the *F8* gene, encoding the coagulation factor VIII (FVIII).[1] HA patients can be treated by the administration of exogenous FVIII. However, the therapy can lead to the development of anti-drug antibodies (ADA) in approximately 30% of severe HA patients, directed against the A2, A3, C1, or C2 domains of the FVIII molecule.[2] These inhibitors are produced in a $CD4^+$ T cell dependent manner, when foreign FVIII peptides are presented on the MHC class II molecules.[3] Additionally, single nucleotide polymorphisms in immune-specific genes such as *TNF-α*, *IL10* and *CTLA-4* play a role in the patient immunogenicity.[4-6]

The *F8* genotype plays a crucial role in inhibitor formation. Among null mutations, large deletions are associated with the highest risk, followed by nonsense mutations and intron 22 inversions (I22I), which result in a complete absence of FVIII protein synthesis.[3] However, the risk of inhibitor development depends also on the type of mutation and their location with the light chain domains being more immunogenic than those located in the heavy chain domains.[3,7,8]

Additionally, *F8* stop mutations in the B domain demonstrated basal readthrough beyond the premature termination codons (PTC), resulting in the synthesis of residual FVIII antigen measured from patient plasma suggesting the presence of non-functional or partially functional protein.[9] Residual truncated FVIII protein in I22I patients was previously detected, by immunohistochemical staining of human I22I liver explant. The missing protein part may be compensated by *F8B*, reasoning the lower risk for inhibitor development.[10] Nevertheless, due to antibody unspecificity, the actual FVIII expression in I22I remains unresolved.[11]

Despite these insights, the mutation-specific molecular mechanisms leading to the higher risk of inhibitors remain poorly understood. While the synthesis of a residual full-length FVIII could lower inhibitor development, the endogenous levels of a truncated protein may alter central or peripheral tolerance causing immunogenicity.[12]

The FVIII protein is synthesized in endothelial cells (EC), such as liver sinusoidal endothelial cells (LSEC), microvascular endothelial cells (MVEC) and lymphatic endothelial cells (LEC).[13-15] However, primary ECs exhibit intrinsic heterogeneity in terms of their proliferation potential, marker expression and functionality.[16] This variability can complicate disease modeling and therapeutic studies. Differentiation of induced pluripotent stem (iPS) cells into more homogenous EC subtypes provides a robust platform to study the synthesis of FVIII.[17,18] Additionally, patient iPS cell derived EC models enable analysis of *F8* mutations on FVIII protein expression and translation reflecting individual genetic variation.

IPS cells were generated from PBMCs of six HA patients with nonsense mutations, one patient with I22I and one with a large deletion in the A2 domain (Figure 1A). The location of the respective mutations within the *F8* gene is illustrated in Figure 1B. Inhibitor history of the reported mutations is summarized in Figure 1C. The patient specific iPS cells were differentiated into iLEC and iLSEC to study endogenous *F8* expression on the mRNA and protein levels. The established cellular model contains all exon-intron boundary junctions capable of reflecting the endogenous mutational framework.

We identified FVIII variants within patient-derived iLEC and iLSEC with nonsense mutations R1960X and R2228X in the light chain and confirmed the existence of an I22I variant in our cellular models. Furthermore, the FVIII nonsense variants were found to co-localize with SEL1L (Suppressor/Enhancer of Lin-12-like) a known facilitator of proteasomal degradation. These results

provide interesting insights into the cellular processing of FVIII variants and could contribute to tackle immunogenicity challenges in HA replacement therapy.

METHODS

Blood samples and reprogramming

Blood samples were collected from eight severe HA-patients and a healthy male control (Cm1). Samples were obtained upon written informed consent. The local ethics committee of the University Clinic of Bonn approved the study (number 244/19)**.** Peripheral blood mononuclear cells (PBMCs) were isolated and reprogrammed as per the previously published protocol.[19]

Differentiation of iPS into iLEC and iLSEC

2D monolayer differentiation from iPS cells into vascular ECs (vEC) was performed according to a published protocol.[20] These cells were further used for downstream applications (Supplementary methods). bFGF and L-685-458 were only added when differentiating into iLSEC. Day 6 angioblasts for both subtypes were seeded at a cell density of $5{,}2x10^4$ cells/cm^2 on tissue culture plates coated with fibronectin.

Differentiation into iLEC: $CD144^+$ angioblasts were maintained in ECGM-MV2 medium supplemented with VEGF-A. Starting day 11 until 14 VEGF-C and IL3 was added (Figure 2 & 3). *Differentiation into iLSEC:* $CD34^+$ angioblasts were maintained under hypoxic conditions (37°C, 5% CO_2, 5% O_2, 95% N_2). Cell medium was a combination of StemPro™-34 and ECGM-MV2 (1:1) supplemented with VEGF-A and bFGF (E/S) or complete ECGM-MV2 medium supplemented with VEGF-A (E). On day 10, LSEC induction (LI) medium was supplemented with SB-431542, 8-Br-cAMP +/- bFGF. Medium was replaced every second day until day 16 (Figure 4 & 5). Characterization and functional assays were conducted.

ELISA

Day 14 iLEC and iLSEC were harvested, counted, and resuspended in NP-40 lysis buffer containing protease inhibitor. Cells were adjusted to a concentration of 1×10^6 cells per 50 µl lysis buffer, and the corresponding volume of buffer was added to the cell pellet. Using our in-house established ELISA, lysates were applied at a 1:6 dilution in triplicates, corresponding to ~1.7×10^5 cells per well. GMA012 (anti-A2) or CaptureSelect™ biotin anti-FVIII conjugate (anti-A3) were used as capture antibodies. SAF8C-HRP was used for detection by luminescence read-out. Quantification was based on a standard curve prepared using HEK *F8*-/- lysate (1:6, as for the samples) combined with recombinant full-length FVIII (Kogenate) (5, 7.5, 10, 20, 40, 80, 160, 320 mU/ml).

Western blot

Lysate of $1x10^7$ differentiated iLSEC was prepared using NP-40 lysis buffer and purified using 50 kD-MW cut-off Vivaspin columns. The purified lysate was incubated with SAF8C-AP or GMA012 for one hour, followed by purification using the CaptureM™ IP & Co-IP kit. Eluted proteins were loaded on 7.5% TGX gel. Western blot was conducted using GMA012 or SAF8C-AP antibody with an overnight incubation at 4°C.

Sample digestion for mass spectrometry (MS)

Purified cell eluents (as used for WB) were subjected to cysteine reduction and alkylation with 20 mM DTT and 40 mM acrylamide in 50 mM triethylammonium bicarbonate (TEAB). A mixture of hydrophilic carboxylate-coated magnetic beads was employed. FVIII protein binding was induced with ethanol. After a brief washing step with ethanol, the bound peptides were subjected to overnight tryptic digestion at 37 °C. Peptide solutions were separated from the magnetic beads, dried and further desalted with C18 ZipTips. (Supplemental methods).

Further information provided in supplementary methods.

RESULTS

Generation of iPS cells from HA-patient-derived PBMCs

PBMCs were isolated from blood and expanded for erythroid progenitor cells. After episomal reprogramming, iPS cell clones appeared between day 9-12 (Figure 1A). We confirmed pluripotency by APLive- and subsequent immunostaining of the stem cell markers Nanog, SSEA-4, Tra-1-60 and Oct4. Ability to differentiate into all three germ layers was confirmed *in vitro* for each clone. (Figures S1 & S2) Silencing of the transgene was validated by endpoint PCR proving the absence of episomal vectors in each iPS cell clone (Figure S1). Genomic integrity was confirmed by SNP-array (Figure S3). CRISPR/Cas9 knockout of *F8* ($F8^{-/-}$) was generated from Cm1 IPS clone (Figure S4).

Enhancing FVIII synthesis in iPS derived EC to improve FVIII detection

iPS cells were differentiated towards the mesodermal lineage (Figure 2), utilizing BMP4 and CHIR, a small molecule inhibitor of WNT signaling. Mesoderm was induced towards a vascular endothelial lineage by introducing high concentrations of VEGF-A (200 ng) and forskolin (Figure S5). On day 6, $CD144^{+}$ ECs were cultured with VEGF-A (10 ng), to direct the cells into a venous lineage. These models were consistently compared against primary (p) ECs, including pHUVEC, pHDLEC and pLSEC. pHDLEC exhibited high *F8* expression, comparable to pLSEC. The lymphatic endothelial cell markers *LYVE1*, *VEGFR-3*, *PROX1* and *PDPN* (*Podoplanin)* were highly expressed in pHDLEC, differing significantly from the pLSEC profile (Figure 3A & S6).

iPS derived vECs established a venous identity with no significant difference in *F8* expression (Figure 3A, A10D & S7A). Treatment with VEGF-C +/- angiopoietin for three additional days directing vECs towards lymphatic cells resulted in an increase in the expression levels of *LYVE1* and *VEGFR-3*. No or low expression of *PROX1*, *PDPN* and *F8* was observed (T1, T2; Figure S7B and C). Inflammatory cytokine IL3 resulted in a 2-fold increase in *F8* expression and upregulation of *COUP-TFII*, *LYVE-1*, *VEGFR-3* and *PROX1*, without notable changes in *PDPN* (Figure 3A, AC3D-IL3-6h, S8). FACS confirmed VEGFR-3 expression in populations treated with both VEGF-C and IL3. CD144 expression was stable under both conditions (Figure 3B). Immunofluorescence (IF) confirmed LEC marker expression of PROX1, COUP-TFII, LYVE1, CD31, CD144 and VWF when treated with a combination of VEGF-A, VEGF-C and IL3 (AC3D IL3-6h, Figure 3C). VEGF-A and VEGF-C treatments over seven days (Figure 3A, AC7D) or in combination with TNFα on days 11 to 13 (Figure 3A, AC7D TNFα 3D) demonstrated no significant changes in *F8.* However, addition of TNFα significantly increased *COUP-TFII* and *PDPN* levels (Figure 3A, AC7D TNFα 3D).

Since LSECs are a known primary site for FVIII synthesis[21], we differentiated iPS cells into LSEC to study the expression of *F8*. We adapted a previously published protocol[17] implementing key modifications (Figure 4). Mesoderm was induced under normoxia. $CD34^+$ MACS selected angioblasts were subjected to hypoxia and maintained until day 10. Two medium conditions to induce a venous subtype were evaluated (materials and methods). For LSEC induction, both media conditions implemented 8-Br-cAMP and TGFβ inhibitor SB-431542 fostering the expression of LSEC markers *STAB2*, *LYVE1* and *FCGR2b.*[17,22] Arterial, venous and LSEC-specific markers were analysed by rtPCR, FACS and IF staining (Figure 5A-C). From lineage tracing studies, it has been established that venous positive population leads to the development of LSEC specification.[23,24] The $CD34^+$ population was confirmed in both treatment conditions (Figure 5B, S9). VEGF-A downregulates notch signalling promoting venous specification with 86.7% $CD73^+$ population (LI-4D E/S) and 74.2% for LI-6D E. Both conditions show a $CD184^{low}$ population due to the combined effect of GSI and notch signalling inhibition. LI-2D E/S demonstrated a 3.3-fold increase in *F8* compared to A10D while longer treatment observed lower expression values (LI-4D E/S) similar to LI-6D E. LI-2D E/S additionally exhibited a significant increase in *COUP-TFII*, *STAB2* and *FCGR2b* expression, while *FCGR2b* maintained a stable expression across all three conditions. *VEGFR3* showed a slight significant increase in LI-2D E/S and LI-4D E/S samples. *PROX1* and *PDPN* expression levels were elevated in all three conditions compared to A10D. *LYVE1* expression was upregulated only under E/S conditions (Figure 5A). IF confirmed the expression of PROX1, COUP-TFII, CD31, LYVE1, STAB2 and VWF in iLSEC (LI-4D E/S, Figure 5C). Treatment with IFNγ confirmed inflammatory responsiveness and increased *CIITA* expression and consequently enhanced MHC-II levels in iLSEC, but also in vEC (A10D) (Figure S10).

Transcript integrity, synthesis and detection of the FVIII protein

We detected full-length *F8 mRNA* in iPS cell-derived vEC from all six patient samples containing premature termination codons (PTCs), indicating presence of normal splicing product when compared to Cm1 (Figure S11). The analysis of *F8 mRNA* in patient sample I22I revealed the expected break between exons 22 and 23 due to the lack of amplification of region D. Nested PCRs designed to span exons 19-24 and 24-26 failed to produce any amplifiable products. Exons 1-8 of rendered region A were not amplified for the patient sample LDA2 (exons 7-9). This absence of PCR products extended to nested regions exons 1-5 and 4-8. No amplification was observed between exons 8-11.

To confirm the synthesis of FVIII, we utilized a robust mass spectrometry-based method for detecting and quantifying proteins. Six unique endogenous peptides from Cm1, with a false discovery rate (FDR) of 1% (Figure 6A, Table S2) were detected. Peptides were identified from multiple domains within the FVIII protein: DFPILPGEIFK and NVILFSVFDENR derived from A2, GELNEHLGLLGYPIR from A3, VDLLAPMIIHGIK from C1, and the peptides SNAWRPQVNNPK and IHPQWVHQIALR from the C2 domain across three separate measurements. These results indicate the integrity and completeness of the synthesized protein. IF was conducted to detect and visualize the low abundant FVIII. Biotin anti-FVIII conjugate was determined to be effective after rigorous evaluation against various FVIII-specific monoclonal antibodies used for IF and ELISA results (data not shown). FVIII was detected in pLSEC and iLSEC, confirming endogenous FVIII synthesis. No signal was detected in the Cm1 $F8^{-/-}$ (Figure 6B).

ELISA measurements were also performed on lysates from iLEC of Cm1, I22I, LDA2 and six nonsense mutations. GMA012 detected FVIII-Ag for both Cm1 and I22I samples, which served as positive controls (Figure 7A). FVIII-Ag was also detected for R1960X and R2228X, when normalized

against LDA2 (negative control). Additionally, iLSEC lysates from Cm1, I22I, Cm1 *F8*$^{-/-}$, LDA2 and nonsense mutations, were analysed, and detected FVIII-Ag in Cm1, I22I, and R1960X and R2228X. Biotin anti-FVIII conjugate confirmed the presence of FVIII in Cm1, while the Cm1 *F8*$^{-/-}$ and LDA2 samples remained negative. FVIII-Ag was also observed for R1960X and R2228X, albeit at different levels.

Molecular characterization of FVIII variants and intracellular processing

To investigate the intracellular expression and processing of FVIII variants, we first performed immunoprecipitation using the polyclonal anti-FVIII antibody SAF8C-AP, followed by Western blot detection with the monoclonal anti-A2 antibody GMA012 (Figure 7B). In Cm1, a strong 250 kDa band and 100-200 kDa smear was observed representing the full-length single-chain FVIII and furin cleaved heavy chain products respectively. I22I showed a distinct single-chain product between 240–250 kDa and faint bands around 160-170 kDa and 110-150 kDa range, suggesting altered processing compared to Cm1. A faint band was observed for R2228X around 240 kDa and 100-130 kDa, suggestive of targeted degradation. R1960X exhibited an extensive smear between 80-230 kDa and a faint signal around 240 kDa, indicating degradation and incomplete processing.

To assess glycosylation and processing, immunoprecipitation using GMA012, detection with SAF8C-AP before and after PNGase F treatment was conducted (Figure 7C). In Cm1, deglycosylation converted the heavy chain bands at 120-200 kDa (left panel) into a sharp band at 160-170 kDa (HC). In addition, glycosylated single-chain product SC^{Glyc} (>260 kDa) shifted to ~250 kDa (SC) following PNGase F treatment (right panel), confirming N-linked glycosylation and processing. I22I displayed two stable bands at ~250 kDa (SC^{mut}) and 160-170 kDa (HC) both before and after PNGase F treatment, without mobility shift, indicating a lack of glycosylation and accumulation of a truncated proteolytic FVIII product in the ER. R2228X variant showed a similar glycosylation-dependent shift of the heavy chain upon treatment as observed in Cm1, while the single chain product (SC^{mut}) remained unchanged. In contrast, R1960X displayed faint SC^{mut} and HC signals with a broad smear that intensified after PNGase F treatment, indicative of instability, misfolding, and impaired deglycosylation, resulting in accumulation of degraded intermediates.

Notably, the banding patterns differ between SAF8C (polyclonal) and GMA012 (monoclonal A2) immunoprecipitation. For I22I, both the 240–250 kDa SC^{mut} and 160–170 kDa HC species are consistently detectable with both antibodies although SAF8C enriches a stronger single chain product and an additional 100–150 kDa product that is not recovered with GMA012, most likely due to the lack of an accessible A2 epitope. For R1960X, SAF8C IP reveals a broad smear of heterogeneous degradation products, whereas GMA012 selectively precipitates only weak A2-containing species with residual signals around 160–170 kDa, indicative of degraded heavy-chain related intermediates.

FVIII and VWF follow distinct trafficking routes in induced and primary endothelial cells

Protein Disulfide Isomerase (PDI), an endoplasmic reticulum (ER) marker, and COPII as a marker for the ER-Golgi intermediate compartment (ERGIC) were used to localize FVIII in iLSEC (Figure 8A, Table S3). FVIII accumulated within the ER with minimal co-localization with COPII, indicating limited secretion and no detectable extracellular FVIII activity (data not shown). Furthermore, no co-

localization of FVIII with von Willebrand Factor (VWF) was observed, suggesting that FVIII and VWF may not be co-synthesized or secreted via shared pathways in this model.

To examine VWF synthesis, we performed VWF immunostaining in the induced models iLSEC and iLEC, as well as in pHUVEC and pHDLEC (Figure S12A). While VWF was detectable in all cell types, only pHDLEC exhibited distinct punctate structures consistent with Weibel-Palade bodies, indicating differential VWF processing in our models. Notably, pHDLEC also showed high *F8* mRNA expression (Figure S12B), but co-staining for FVIII and VWF revealed no co-localization (Figure S12C). This finding contrasts with reports from primary LEC, where FVIII and VWF have been shown to co-localize.[25]

Immunofluorescent staining identifies FVIII variant R1960X in ER degradative pathway

We aimed to elucidate the processing of FVIII variants, especially in the context of degradation and immunogenicity. Co-staining experiments were conducted to assess the localization and potential fate of wild-type and variant forms of FVIII (Biotin anti-FVIII conjugate) within the ER. Wild type (Cm1) and both FVIII variants R1960X & R2228X highly co-localized with PDI with a Pearson´s correlation coefficient (PCC) of 0.6, indicating their presence within the ER (Figure 8B). For I22I, a significant reduction in co-localization (PCC = 0.4) was observed. BiP, an ER chaperone, also co-localized with FVIII wild-type and nonsense mutation R1960X (PCC = 0.5; Figure 8B), and to a lower extend with R2228X (PCC = 0.3) implying an involvement of BiP in the folding and processing of FVIII variants within the ER. Notably, the co-localization was significantly low for the I22I variant (PCC = 0.2). SEL1L, a marker for the ER-associated degradation (ERAD-L) pathway, was found to co-localize with the FVIII variant R1960X (PCC = 0.38) and R2228X (PCC = 0.32), but not with Cm1 or I22I (PCC = 0.2; Figure 8B). The co-localization of SEL1L with both nonsense variants suggests that the FVIII protein is targeted for proteasomal degradation, although to differing extents, with only R1960X showing statistically significant co-localization compared to wild type.
In addition to these experimental observations, we performed *in silico* predictions of peptide presentation based on the patients' HLA genotypes (Table S4). These exploratory analyses indicated that R1960X may present a higher number of FVIII-derived peptides via HLA-B (MHC-I) as well as HLA-DRB1 and HLA-DQA1/DQB1 (MHC-II) compared to R2228X (Figures S13 & S14).

DISCUSSION

A strong correlation exists between the type of *F8* mutation and consequently the residual amount of intracellular protein from null mutations that influences the risk for inhibitor development.[8] Thus, we asked ourselves whether truncated parts of the endogenous FVIII protein being produced could influence the immunogenicity against replacement therapy in HA patients. Since the FVIII protein is synthesized and located within sinusoidal and lymphatic ECs,[13,14,26] we established two patient-specific iPS-based EC models: iLEC and iLSEC capable of producing FVIII to answer this question.

Differentiation towards iLEC involved treatment of vECs to elevate lymphangiogenesis. VEGF-C and angiopoietin are known regulators of lymphatic markers such as *LYVE1*, *VEGFR3, PROX1 and PDPN.*[27,28] Although upregulation of *LYVE1* and *VEGFR3* was achieved, we observed varied to no expression in *PROX1* and *PDPN*. Our optimized model combining VEGF-A, VEGF-C, and IL-3 treatments, resulted in a 2.3-fold increase in *F8* expression. We also modulated lymphangiogenesis by the NF-kB pathway, since *PROX1* and *VEGFR3* are downstream targets, by testing the

inflammatory cytokines.[29] In this approach, a significant upregulation of *F8* expression was observed only in the presence of IL3, suggesting its unique role in promoting *F8* expression. We also observed an antagonistic effect of TNFα on *LYVE1* expression, suggesting LYVE1 a role as gatekeeper that restricts leukocyte trans-lymphatic migration under non-inflammatory conditions.[30] Treatment with IFNγ led to the upregulation of MHC-II molecules, facilitated by the induction of the CIITA transcription factor.[31] The varied responses to different cytokines highlight the inherent complexity of cytokine signaling in endothelial cells and underscore the importance of considering multiple pathways and interactions when designing strategies to enhance *F8* expression in an immune-modulatory context. All patient-specific variants were subsequently analysed using ELISA in the iLEC model, where the first detectable pattern revealed the presence of not only Cm1 and I22I, but also the two light chain variants R1960X and R2228X.

$CD144^+$ cells are considered more mature and committed to endothelial cell lineages involved in lymphatic vascular formation. Interestingly, there is evidence that LSECs arise from a haematopoietic stem cell source during development.[32] This is likely due to shared developmental pathways between endothelial and haematopoietic lineages during mesodermal differentiation through the haemangioblast, which gives rise to both blood cells and endothelial cells.[32-34] Therefore, differentiation towards iLSEC was established by selection of $CD34^+$ angioblasts upon notch signaling inhibition. In the presence of hypoxia, progenitors were maintained in VEGF-A and TGF-β inhibition which led to a 3.3-fold increase of *F8* expression and up-regulation of LSEC-specific markers *STAB2*, *FCGR2b* and *LYVE1*. The FVIII positive samples initially detected in the iLEC model were confirmed in the iLSEC model, and all subsequent downstream analyses were conducted using the iLSEC model.

Recent single-cell RNA sequencing studies have highlighted the intrinsic heterogeneity of primary LSECs, which show zonation-dependent differences in marker expression and function.[33] For instance, central venous LSECs typically express *STAB2*, *LYVE1*, *FCGR2b* and *F8* but lack *VWF*, whereas periportal LSECs express *VWF* and *F8* but show reduced levels of these canonical LSEC markers. Consistent with these findings, qRT-PCR analysis revealed that our primary LSECs expressed *F8* but lacked detectable levels of *STAB2* or *FCGR2b*, suggesting a periportal phenotype (Zone 1), whereas our iPSC-derived LSECs appear to represent a more central venous phenotype (Zone 2/3) with stable *STAB2*, *LYVE1* and *FCGR2b* expression after two days of LSEC induction (LI-2D E/S; Figure 5A).

There is evidence that LSECs with high *F8* expression often exhibit low *VWF* expression, suggesting an inverse relationship between these two proteins within specific endothelial subpopulations.[13] In our study, we observed no co-localization of FVIII and VWF in neither the iPSC-derived endothelial model (iLSEC) nor in primary HDLEC. Specifically, only the pHDLEC displayed mature Weibel-Palade bodies as indicated by the distinct VWF staining pattern. In contrast, VWF localization in the iPSC-derived endothelial cells appeared immature and diffuse, lacking typical storage structures. To our knowledge, little is known about the intracellular co-localization dynamics of FVIII and VWF in liver endothelial cells. A single study reported FVIII localization within Weibel-Palade bodies in primary LECs, but our data do not support this observation.[25] Further research is needed to elucidate whether this spatial separation reflects functional divergence or different maturation stages of endothelial subtypes.

While central tolerance is key role in FVIII tolerance[35], peripheral tolerance may be responsible for the existence of anti-FVIII antibodies in healthy individuals.[36,37] Peripheral *F8* expression by non-haematopoietic antigen presenting cells (nhAPC) like LECs and LSECs, might be crucial in mediating tolerance to FVIII through immune-modulatory mechanisms such as T-cell deletion,

anergy, or induction of regulatory T-cells via TGF-β and Notch signaling. LECs present self-proteins via MHC-I in an AIRE-independent manner and promoting tolerance by PD1/PD-L1.[38] Presentation of self-proteins by MHC-II was only reported after transfer to dendritic cells.[39] Similarly, LSECs can engage $CD8^+$ T cells via endogenous antigen presentation.[40,41]

In nhAPCs, MHC-I presents peptides generated by the ubiquitin-proteasome system (UPS).[42] During ER-associated degradation (ERAD), misfolded polypeptides are transported out of the ER lumen to be processed by the UPS. The resulting peptides are then transferred back to the ER and loaded onto TAP for presentation by MHC-I.[43] ERAD-L pathway degrades luminal, aberrantly glycosylated proteins like FVIII.[44] SEL1L is a large ER-luminal receptor that recognizes misfolded substrates via BiP and regulates the ER transmembrane ubiquitin ligase HRD1/gp78, which mediates the first interaction with the UPS during ERAD-L.[45,46]

We also performed *in silico* predictions of peptide presentation based on the HLA genotypes of the three protein-positive patients. These exploratory analyses indicated that patient R1960X, who developed an inhibitor, may present a higher number of FVIII-derived peptides via HLA-B (MHC-I) as well as HLA-DRB1 and HLA-DQA1/DQB1 (MHC-II) compared to patients R2228X or I22I. Furthermore, R1960X displayed a DRB1 repertoire enriched for B-domain peptides, whereas such peptides were not predicted for R2228X and I22I. This observation does not contradict our model in which increased proteasomal degradation of truncated FVIII in R1960X could enhance the supply of peptides for MHC presentation, as suggested by the extensive smear pattern in western blot analyses. At the same time, it must be emphasized that these findings are exploratory: binding and processing predictions reflect algorithmic estimates and inherent database biases, and do not demonstrate actual surface presentation or immunogenicity in vivo (Figures S13 & S14).

Immunofluorescence revealed co-localization of FVIII variant R1960X with SEL1L and BiP demonstrating proteasomal degradation via the ERAD-L pathway. For this patient (R1960X), two immunomodulatory mechanisms may be considered: i: Under normal physiological conditions FVIII is presented by MHC-I to $CD8^+$ T-Cells. Regulatory $CD8^+$ T-cells ($CD8^+CD25^+FoxP3^+$) modulate immune responses by directly suppressing $CD4^+$ effector T-cells in a MHC-class Ib (Qa-1 in mice & HLA-E in humans) dependent pathway.[47-49] Conversely, the truncated FVIII variant might present altered peptide pattern disrupting the suppressive environment. ii: unfolded protein response (UPR) is triggered compromising the tolerogenic functions of LEC and LSEC shifting their cytokine secretion profiles toward inflammation.[50]

The nonsense variant R2228X localized to the ER and exhibited moderate co-localization with both SEL1L and BiP, suggesting partial involvement of the ERAD-L pathway. Additionally, the western blot pattern of R2228X resembled that of the wild-type protein more closely than R1960X, implying a potential for partial secretion. Notably, the patient harboring the R2228X variant did not develop an inhibitor, raising the question of whether residual secretion or limited degradation of the variant protein might contribute to immune tolerance.

In contrast, the I22I variant co-localized with the ER marker PDI, but showed no significant co-localization with SEL1L or BiP, indicating its retention within the ER without effective engagement of the ERAD-L pathway or proteasomal degradation. This suggests that the truncated protein does not efficiently engage classical quality control mechanisms within the ER. The truncated product might be sequestered in a non-functional, aggregated form, which could lead to ER crowding.

In future investigations, it will be crucial to understand specific MHC-I peptide patterns and cytokine secretion profiles associated with wild-type versus FVIII variants. The nonsense mutation patient

specific model enables us to explore PTCs, apart from its surrounding sequence-context. It would be interesting to determine read-through response in combination with patient-specific NMD machinery and explore the differences in degradation mechanisms of the mutated *F8* transcript among HA patients. Additionally, it remains to be clarified whether the chronic ER retention of I22I–derived truncated FVIII contributes to cellular stress, immune activation or tolerance induction.

In conclusion, we established a patient-specific HA cellular model for the endogenous detection of FVIII. By this we detected and localized for the first time endogenous FVIII light chain PTC variants R1960X and R2228X. Additionally, we confirmed the existence of an I22I-derived FVIII variant. Our findings suggest that the differential processing and intracellular localization of FVIII variants, particularly the interaction with the ERAD-L pathway, may contribute to the hierarchical risk of inhibitor formation. This underscores the need for further investigation into patient-specific FVIII variants and their immunogenic potential, especially in relation to antigen presentation and regulatory T-cell function.

Limitations of the study

Detection of the FVIII protein especially in its functional secreted form has been challenging. While our attempt in detecting intracellular FVIII protein was successful, the secretory pathways might not be fully represented in vitro. Finally, while patient derived iPS cells are extremely valuable, we cannot generalize the findings of this study across all HA patients and genotypes. This can be attributed to individual genetic and epigenetic variability.

REFERENCES
Stability and Proteasomal Targeting of LC F8 PTC

1. Franchini M, Mannucci PM. Past, present and future of hemophilia: a narrative review. Orphanet J Rare Dis. 2012;7:24.
2. Garagiola I, Palla R, Peyvandi F. Risk factors for inhibitor development in severe hemophilia a. Thromb Res. 2018;168:20-27.
3. Oldenburg J, Pavlova A. Genetic risk factors for inhibitors to factors VIII and IX. Haemophilia. 2006;12(6):15-22.
4. Astermark J, Oldenburg J, Carlson J, et al. Polymorphisms in the TNFA gene and the risk of inhibitor development in patients with hemophilia A. Blood. 2006;108(12):3739-3745.
5. Astermark J, Oldenburg J, Pavlova A, Berntorp E, Lefvert AK, Group MS. Polymorphisms in the IL10 but not in the IL1beta and IL4 genes are associated with inhibitor development in patients with hemophilia A. Blood. 2006;107(8):3167-3172.
6. Astermark J, Wang X, Oldenburg J, Berntorp E, Lefvert AK, Group MS. Polymorphisms in the CTLA-4 gene and inhibitor development in patients with severe hemophilia A. J Thromb Haemost. 2007;5(2):263-265.
7. David D, Santos IM, Johnson K, Tuddenham EGD, McVey JH. Analysis of the consequences of premature termination codons within factor VIII coding sequences. J Thromb Haemost. 2003;1(1):139-146.
8. Gouw SC, van den Berg HM, Oldenburg J, et al. F8 gene mutation type and inhibitor development in patients with severe hemophilia A: systematic review and meta-analysis. Blood. 2012;119(12):2922-2934.
9. Testa MF, Lombardi S, Bernardi F, et al. Translational readthrough at F8 nonsense variants in the factor VIII B domain contributes to residual expression and lowers inhibitor association. Haematologica. 2023;108(2):472-482.
10. Pandey GS, Yanover C, Miller-Jenkins LM, et al. Endogenous factor VIII synthesis from the intron 22-inverted F8 locus may modulate the immunogenicity of replacement therapy for hemophilia A. Nat Med. 2013;19(10):1318-1324.
11. Vir P, Gunasekera D, Dorjbal B, et al. Lack of factor VIII detection in humans and dogs with an intron 22 inversion challenges hypothesis regarding inhibitor risk. J Thromb Haemost. 2024;22(12):3415-3430.
12. Bernabeu-Herrero ME, Patel D, Bielowka A, et al. Mutations causing premature termination codons discriminate and generate cellular and clinical variability in HHT. Blood. 2024;143(22):2314-2331.
13. Pan J, Dinh TT, Rajaraman A, et al. Patterns of expression of factor VIII and von Willebrand factor by endothelial cell subsets in vivo. Blood. 2016;128(1):104-109.
14. Jacquemin M, Neyrinck A, Hermanns MI, et al. FVIII production by human lung microvascular endothelial cells. Blood. 2006;108(2):515-517.
15. Shahani T, Lavend'homme R, Luttun A, Saint-Remy JM, Peerlinck K, Jacquemin M. Activation of human endothelial cells from specific vascular beds induces the release of a FVIII storage pool. Blood. 2010;115(23):4902-4909.
16. Koch PS, Lee KH, Goerdt S, Augustin HG. Angiodiversity and organotypic functions of sinusoidal endothelial cells. Angiogenesis. 2021;24(2):289-310.
17. Gage BK, Liu JC, Innes BT, et al. Generation of Functional Liver Sinusoidal Endothelial Cells from Human Pluripotent Stem-Cell-Derived Venous Angioblasts. Cell Stem Cell. 2020;27(2):254-269.e259.

18. Koui Y, Kido T, Ito T, et al. An In Vitro Human Liver Model by iPSC-Derived Parenchymal and Non-parenchymal Cells. Stem Cell Rep. 2017;9(2):490-498.
19. Jamil MA, Singer H, Al-Rifai R, et al. Molecular Analysis of Fetal and Adult Primary Human Liver Sinusoidal Endothelial Cells: A Comparison to Other Endothelial Cells. Int J Mol Sci. 2020;21(20):7776.
20. Patsch C, Challet-Meylan L, Thoma EC, et al. Generation of vascular endothelial and smooth muscle cells from human pluripotent stem cells. Nat Cell Biol. 2015;17(8):994-1003.
21. Fahs SA HM, Shi Q, Weiler H, Montgomery RR. A conditional knockout mouse model reveals endothelial cells as the principal and possibly exclusive source of plasma factor VIII. Blood. 2014;123(24):3706-3713.
22. Arai T, Sakurai T, Kamiyoshi A, et al. Induction of LYVE-1/stabilin-2-positive liver sinusoidal endothelial-like cells from embryoid bodies by modulation of adrenomedullin-RAMP2 signaling. Peptides. 2011;32(9):1855-1865.
23. Hen G, Nicenboim J, Mayseless O, et al. Venous-derived angioblasts generate organ-specific vessels during zebrafish embryonic development. Development. 2015;142(24):4266-4278.
24. Zhang H, Pu W, Tian X, et al. Genetic lineage tracing identifies endocardial origin of liver vasculature. Nat Genet. 2016;48(5):537-543.
25. Hough C, Notley C, Mo A, Videl B, Lillicrap D. Heterogeneity and reciprocity of FVIII and VWF expression, and the response to shear stress in cultured human endothelial cells. J Thromb Haemost. 2022;20(11):2507-2518.
26. Shahani T, Covens K, Lavend'homme R, et al. Human liver sinusoidal endothelial cells but not hepatocytes contain FVIII. J Thromb Haemost. 2014;12(1):36-42.
27. Lee SJ, Park C, Lee JY, et al. Generation of pure lymphatic endothelial cells from human pluripotent stem cells and their therapeutic effects on wound repair. Sci Rep. 2015;5:11019.
28. Rufaihah AJ, Huang NF, Kim J, et al. Human induced pluripotent stem cell-derived endothelial cells exhibit functional heterogeneity. Am J Transl Res. 2013;5(1):21-35.
29. Flister MJ, Wilber A, Hall KL, et al. Inflammation induces lymphangiogenesis through up-regulation of VEGFR-3 mediated by NF-kappaB and Prox1. Blood. 2010;115(2):418-429.
30. Johnson LA, Prevo R, Clasper S, Jackson DG. Inflammation-induced uptake and degradation of the lymphatic endothelial hyaluronan receptor LYVE-1. J Biol Chem. 2007;282(46):33671-33680.
31. Steimle V, Siegrist CA, Mottet A, Lisowska-Grospierre B, Mach B. Regulation of MHC class II expression by interferon-gamma mediated by the transactivator gene CIITA. Science. 1994;265(5168):106-109.
32. Ditadi A, Sturgeon CM. Directed differentiation of definitive hemogenic endothelium and hematopoietic progenitors from human pluripotent stem cells. Methods. 2016;101:65-72.
33. MacParland SA, Liu JC, Ma XZ, et al. Single cell RNA sequencing of human liver reveals distinct intrahepatic macrophage populations. Nat Commun. 2018;9(1):4383.
34. Scarfo R, Randolph LN, Abou Alezz M, et al. CD32 captures committed haemogenic endothelial cells during human embryonic development. Nat Cell Biol. 2024;26(5):719-730.
35. Madoiwa S, Yamauchi T, Kobayashi E, et al. Induction of factor VIII-specific unresponsiveness by intrathymic factor VIII injection in murine hemophilia A. J Thromb Haemost. 2009;7(5):811-824.
36. Meunier S, Menier C, Marcon E, Lacroix-Desmazes S, Maillere B. CD4 T cells specific for factor VIII are present at high frequency in healthy donors and comprise naive and memory cells. Blood Adv. 2017;1(21):1842-1847.

37. Porcheddu V, Lhomme G, Giraudet R, Correia E, Maillere B. The self-reactive FVIII T cell repertoire in healthy individuals relies on a short set of epitopes and public clonotypes. Front Immunol. 2024;15:1345195.
38. Rouhani SJ, Eccles JD, Tewalt EF, Engelhard VH. Regulation of T-cell Tolerance by Lymphatic Endothelial Cells. J Clin Cell Immunol. 2014;5:1000242.
39. Dubrot J, Duraes FV, Potin L, et al. Lymph node stromal cells acquire peptide-MHCII complexes from dendritic cells and induce antigen-specific CD4(+) T cell tolerance. J Exp Med. 2014;211(6):1153-1166.
40. Knolle PA, Wohlleber D. Immunological functions of liver sinusoidal endothelial cells. Cell Mol Immunol. 2016;13(3):347-353.
41. Xu X, Jin R, Li M, et al. Liver sinusoidal endothelial cells induce tolerance of autoreactive CD4+ recent thymic emigrants. Sci Rep. 2016;6:19861.
42. ten Broeke T, Wubbolts R, Stoorvogel W. MHC class II antigen presentation by dendritic cells regulated through endosomal sorting. Cold Spring Harb Perspect Biol. 2013;5(12):a016873.
43. Blum JS, Wearsch PA, Cresswell P. Pathways of antigen processing. Annu Rev Immunol. 2013;31:443-473.
44. Berner N, Reutter KR, Wolf DH. Protein Quality Control of the Endoplasmic Reticulum and Ubiquitin-Proteasome-Triggered Degradation of Aberrant Proteins: Yeast Pioneers the Path. Annu Rev Biochem. 2018;87:751-782.
45. Christianson JC, Ye Y. Cleaning up in the endoplasmic reticulum: ubiquitin in charge. Nat Struct Mol Biol. 2014;21(4):325-335.
46. Mueller B, Lilley BN, Ploegh HL. SEL1L, the homologue of yeast Hrd3p, is involved in protein dislocation from the mammalian ER. J Cell Biol. 2006;175(2):261-270.
47. Wang YM, Alexander SI. CD8 regulatory T cells: what's old is now new. Immunol Cell Biol. 2009;87(3):192-193.
48. Jiang H, Wu Y, Liang B, et al. An affinity/avidity model of peripheral T cell regulation. J Clin Invest. 2005;115(2):302-312.
49. Jiang H, Chess L. The specific regulation of immune responses by CD8+ T cells restricted by the MHC class Ib molecule, Qa-1. Annu Rev Immunol. 2000;18:185-216.
50. So JS. Roles of Endoplasmic Reticulum Stress in Immune Responses. Mol Cells. 2018;41(8):705-716.

FIGURE TITLES AND LEGENDS

Figure 1. Reprogramming timeline and overview of Hemophilia A patient samples
A. Schematic overview of the reprogramming workflow. Patient-derived PBMCs were expanded in StemSpan™ medium for 8–10 days before electroporation with Epi5™ episomal vectors containing reprogramming factors. Following reprogramming, cells were cultured in ReproTeSR™ medium for 12 days before colonies were picked for clonal expansion (mTeSR™) and quality control. iPSC lines were generated from one healthy male control and eight patients with severe Haemophilia A.

B. Overview of patient-specific FVIII mutations. The panel shows schematic representations of the *F8* gene with the positions of nonsense mutations (PTCs), an intron-22 inversion (I22I), and a large deletion (LDA2). Mutations are grouped by location in the heavy chain (top) or light chain (bottom). Mutations associated with a history of inhibitor development are indicated with (i). Red triangles represent PTC positions within corresponding exon.

C. Reported cases of HA-patients with nonsense mutation (grey) and their associated inhibitor incidences (red) demonstrating PTCs located in the region coding for FVIII light chain (aa1648-2332) have a higher risk for FVIII inhibitors than PTCs located in regions coding for the heavy chain (aa1-aa741) [data generated by FVIII mutation data base www.factorVIII-db.org].

Figure 2: Differentiation of iPSCs into vascular and lymphatic endothelial cell models (vEC/iLEC)
iPS cells were directed into mesodermal lineage using CHIR and BMP4. After a medium switch on day 4 cells were differentiated into vascular endothelial cells (vECs). Cells were either maintained in the presence of low VEGF-A or combined with 100 ng VEGF-C and 50 ng IL3 to achieve iLEC fate.

Figure 3: Specification analysis of iPSC derived vascular and lymphatic endothelial cell models (vEC/iLEC)

A. rt-PCR analysis of cell specific markers in vEC (A10D) and iLEC using *F8*, *COUP-TFII*, *LYVE1*, *VEGFR-3*, *PROX1* and *PDPN*. Maintenance of cells in ECGM-MV2 after CD144 MACS isolation on Day 6: A10D: adding 10 days VEGF-A (Day 6-16) ; AC7D: adding 7 days VEGF-A & VEGF-C (Day 6-13) ; AC7D TNF-α: adding 7 days VEGF-A & VEGF-C (Day 6-13) with 3 days cytokine stimulation using TNF-α (Day 10-13) ; AC3D IL3-6h: adding 5 days VEGF-A (Day 6-11), adding 3 days VEGF-C & VEGF-A (Day 11-14), on Day 14 cytokine stimulation for 6h with IL3; pHUVEC: human umbilical vein endothelial cell ; pHUAEC: human umbilical arterial endothelial cell ; pHDLEC: human dermal lymphatic endothelial cell ; pLSEC: liver sinusoidal endothelial cell. n=200,000 cells. Unpaired t-test significance: *:p<0.05, **:p<0.01, ***:p<0.001, ****:p<0.0001. Results demonstrated as a fold change to pHUVEC.

B. Flow cytometry analysis of CD144 and VEGFR3 surface expression in vEC and iLEC. n = 500,000 cells. Expression is shown percentage of positive populations.

C. Immunostaining of iLEC (AC3D IL3-6h) differentiated cells. Lymphatic marker PROX1 (green) and LYVE1 (red). Venous marker COUP-TFII (green). General EC Marker CD31 (red), CD144 (green) and VWF (red). Nuclei were counterstained in DAPi. Images were acquired using an Axio Observer 7 microscope with ApoTome.2. The objective used was a Plan-Apochromat 20x/0,8 M27. Images were captured with an AxioCam 702 Mono camera. Results depicted as a representative image of biological triplicates.

Figure 4: Differentiation of iPSCs into liver sinusoidal endothelial cell model (iLSEC).
Timeline for differentiation of iPS cells into iLSEC was identical to vEC until day 6 except the presence of GSI for directed differentiation towards the venous lineage (day 4-6). $CD34^+$ cells were MACS isolated. Cells were further maintained for four days in low VEGF-A conditions and induced for the LSEC fate. Starting day 10, LSEC induction (LI) started, and cells were maintained in hypoxia.

Figure 5: Specification analysis of iPSC derived liver sinusoidal endothelial cell models (iLSEC)

A. rt-PCR analysis of cell specific markers in vEC (A10D) and iLSEC using *F8*, *COUP-TFII*, *FCGR2b*, *Stab2*, *LYVE1*, *VEGFR-3*, *PROX1* and *PDPN*. LI-2D E/S: 2 days LI ; 1:1 ECGM-MV2 & StemPro-34 ; LI-4D E/S: 4 days LI ; 1:1 ECGM-MV2 & StemPro-34 ; LI-6D E: 6 days LI, only ECGM-MV2. E/S medium conditions consist of bFGF. Cells cultured in medium condition E does not contain bFGF. A10D: from generic vEC protocol, adding 10 days VEGF-A (Day 6-10). pHUVEC: human umbilical vein endothelial cell ; HUAEC: human umbilical arterial endothelial cell; pHDLEC: human dermal lymphatic endothelial cell; pLSEC: liver sinusoidal endothelial cell. n = 200,000 cells. Unpaired t-test significance: *:p<0.05, **:p<0.01, ***:p<0.001, ****:p<0.0001. All data points indicate mechanical duplicates. Results demonstrated as a fold change to pHUVEC.

B. Flow cytometry analysis of endothelial surface markers KDR and CD34, and of venous and arterial $CD34^+$ subpopulations defined by venous marker CD73 (purple), arterial marker CD184 (pink) and dual positive (black) cells in iLSEC. n = 500,000 cells. Data shown as percentage of positive populations.

C. Immunostaining results of LI-6D E treated cells for PROX1 (green), COUP-TFII, CD31, LYVE1, STAB2, and VWF (all red). Nuclei were counterstained with DAPi. Images were acquired using an Axio Observer 7 microscope with ApoTome.2. The objective used was a Plan-Apochromat 20x/0,8 M27. Images were captured with an AxioCam 702 Mono camera. Results depicted as a representative image of biological triplicates.

Figure 6: Detection of endogenous FVIII protein in wild-type iLSEC by LC/MS and IF
A. List of targeted LC/MS measurements of endogenous FVIII peptides identified by mass spectrometry (n = 6). Biological duplicates of healthy donor.

B. Immunostaining with biotin anti-FVIII conjugate targeting the A3 domain of FVIII visualized with Streptavidin488 (green) in primary LSEC (pLSEC) and iPS derived LSEC (iLSEC) iLSEC Cm1: wild type, iLSEC $F8^{-/-}$: *F8* knockout. Nuclei were counterstained with DAPi. Images were acquired using an Axio Observer 7 microscope with ApoTome.2. The objective used was a Plan-Apochromat 40x/1.4 Oil DIC M27. Images were captured with an AxioCam 702 Mono camera. Results depicted as a representative image of biological triplicates.

Figure 7: Intracellular detection of FVIII protein variants and N-glycosylation status in iPSC-derived endothelial cells
A. ELISA quantification of FVIII antigen in iLEC and iLSEC using anti-FVIII-A2 (GMA012) and anti-FVIII-A3 (biotin anti-FVIII conjugate). Results show detectable FVIII antigen in wild-type (Cm1) and selected mutant variants (I22I, R1960X, R2228X), with lower levels in F8 (–/–) or LDA2 negative controls, confirming intracellular FVIII expression in iPSC-derived endothelial cells.

B. Western blot analysis of immunoprecipitated FVIII protein using SAF8C-AP (IP) and GMA012 (WB). Cell lysates (1x 10^7 cells/sample) from wild-type control (Cm1), I22I, R2228X, R1960X and F8KO were analysed. Molecular weight marker is shown on the left. Results are representative of biological duplicates. The full-length wild-type single-chain FVIII (~250 kDa) is marked with a red asterisk, and the furin-cleaved heavy chain (100 - 200 kDa) with a red bracket. The blue asterisk indicates the I22I single-chain product (240 - 250 kDa); the blue triangle (160 - 170 kDa) and blue bracket (110 - 150 kDa) mark additional faint bands. The R2228X single-chain product (~240 kDa) is marked with a pale-pink asterisk, and the pale-pink bracket highlights a faint band between 100–130 kDa. The R1960X single-chain product (~240 kDa) is indicated by a cyan asterisk, while the cyan bracket marks the broad smear between 80–230 kDa. The FVIII-knockout control (F8KO) showed no signal.

C. Western blot analysis of immunoprecipitated FVIII protein using GMA012 (IP) and SAF8C-AP (WB) before and after PNGase F treatment. Cell lysates (1x10^7 cells/sample) from wild-type control (Cm1), I22I, R2228X and R1960X were analysed. Molecular weight marker is shown on the left. Results are representative of one single experiment. In Cm1, the glycosylated single-chain FVIII (SC^{Glyc}, >260 kDa) and heavy-chain species (HC, 120–200 kDa) are indicated by red asterisks and red brackets. After PNGase F treatment, the single-chain product shifts to ~250 kDa and the heavy-chain converts into a sharp band at 160–170 kDa, marked by a red triangle. The I22I variant shows two stable bands at ~250 kDa (SC^{mut}, blue asterisk) and 160–170 kDa (HC, blue triangle), both unchanged after PNGase F digestion. The R2228X variant displays a single-chain product above 250 kDa (pale-pink asterisk) and a heavy-chain region between 120–200 kDa (pale-pink bracket) that collapses into a distinct band after PNGase F treatment. The R1960X variant is marked with cyan asterisks and cyan triangles, showing faint single- and heavy-chain signals with a broad smear that intensifies after PNGase F treatment.

Figure 8: Subcellular localization and ER retention of wild-type and mutant FVIII in iLSEC.
A. FVIII wild type (green) is co-localizing with ER-Marker PDI (red) showing a mean pearson correlation coefficient (PCC) of 0.6 (left panel). Minimal co-localization was observed between FVIII and individual COPII vesicles with mean PCC of 0.3 (middle panel). Co-localization between FVIII and VWF was mostly absent showing mean PCC of 0.1 (left panel). Nuclei were counterstained with DAPi. Results depicted as a representative image of biological triplicates.

B. Comparison of the intracellular localization of wild-type (Cm1) and mutant FVIII (I22I, R1960X, R2228X) variants in iLSEC. Co-localization of FVIII (green) was analysed with PDI (red, top row), BiP (red, middle row), and SEL1L (red, bottom row). The nuclei are counterstained with DAPi (blue). FVIII with PDI (top row) indicates significant ER retention for Cm1, R1960X and R2228X with mean PCCs of 0.6 and reduction of co-localization for I22I with mean PCC of 0.4 in the corresponding boxplot. FVIII with BiP (middle row) demonstrates co-localization for Cm1, R1960X with mean PCC of 0.5 and R2228X with mean PCC of 0.3. Co-localization for I22I and BiP was absent with mean PCC of 0.2. SEL1L (bottom row) presents absence of co-localization with Cm1 or I22I presenting a mean PCC of 0.2. When normalized to wild type Cm1, both nonsense variants R1960X and R2228X show an increase of co-localization with mean PCCs of 0.38 and 0.32. Images were acquired using an Axio Observer 7 microscope with ApoTome.2. The objective used was a Plan-Apochromat 40x/1.4 Oil DIC M27. Images were captured with an AxioCam 702 Mono camera. Results depicted as a representative image of biological triplicates.

Figure 1

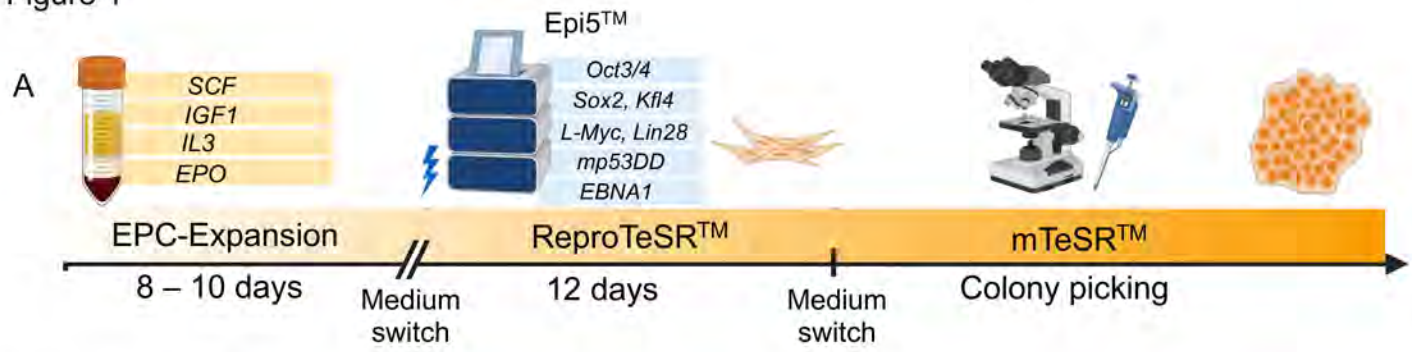
A
SCF
IGF1
IL3
EPO
Epi5™
Oct3/4
Sox2, Klf4
L-Myc, Lin28
mp53DD
EBNA1
EPC-Expansion
8 – 10 days
Medium switch
ReproTeSR™
12 days
Medium switch
mTeSR™
Colony picking

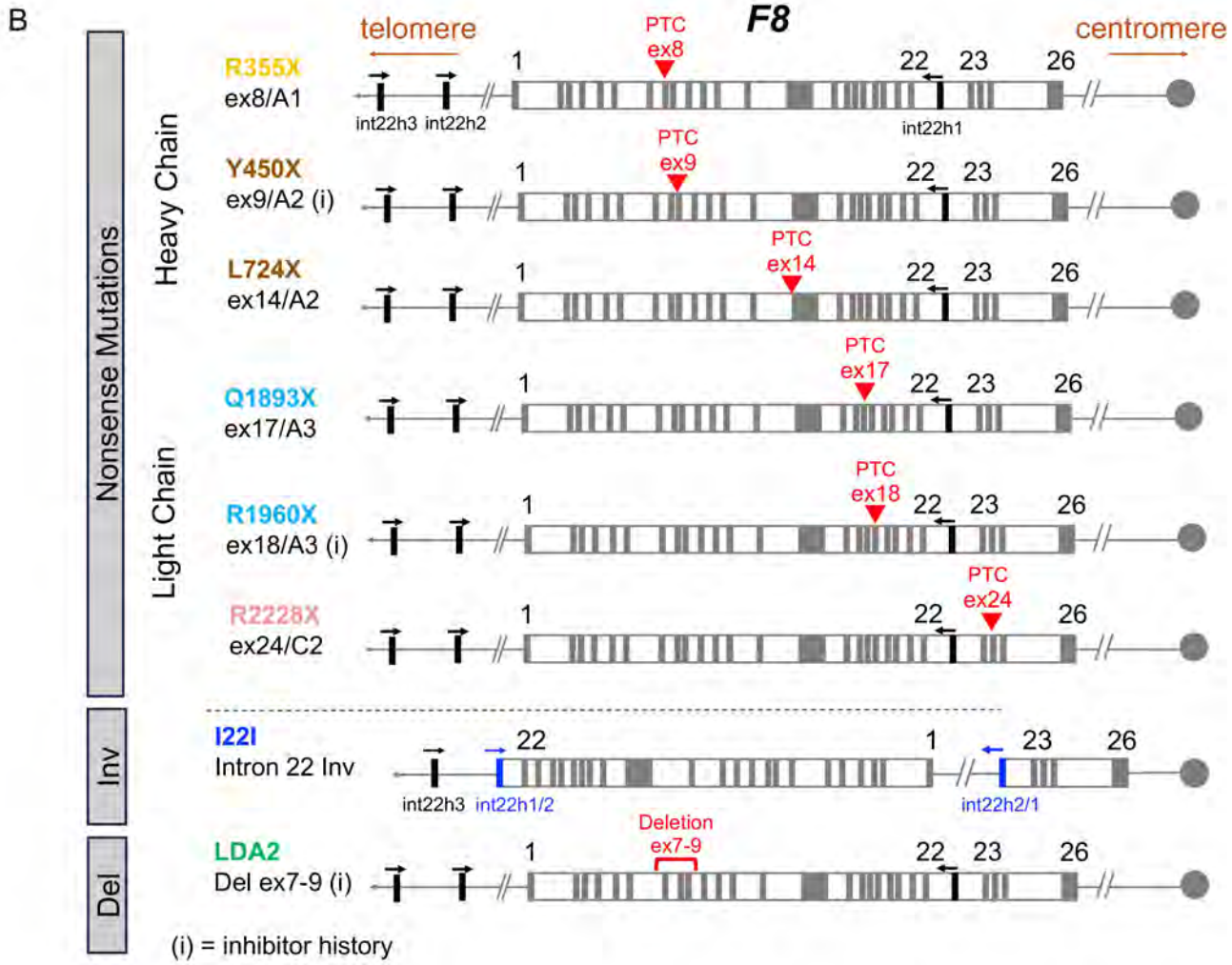
B
F8
telomere
centromere
Nonsense Mutations
Heavy Chain
Light Chain
Inv
Del
R355X
ex8/A1
PTC ex8
int22h3 int22h2
int22h1
Y450X
ex9/A2 (i)
PTC ex9
L724X
ex14/A2
PTC ex14
Q1893X
ex17/A3
PTC ex17
R1960X
ex18/A3 (i)
PTC ex18
R2228X
ex24/C2
PTC ex24
I22I
Intron 22 Inv
int22h3 int22h1/2
int22h2/1
LDA2
Del ex7-9 (i)
Deletion ex7-9
(i) = inhibitor history

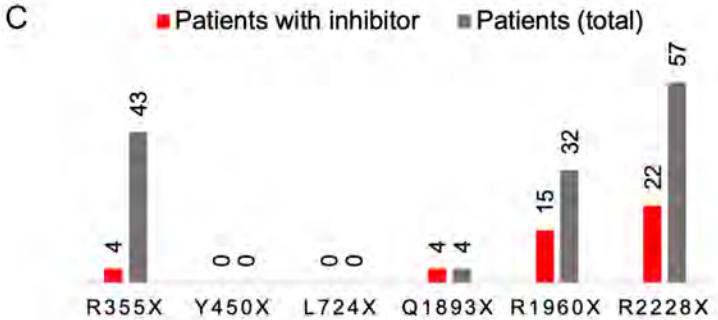
C
Patients with inhibitor
Patients (total)
4
43
0
0
0
0
4
4
15
32
22
57
R355X
Y450X
L724X
Q1893X
R1960X
R2228X

Figure 2

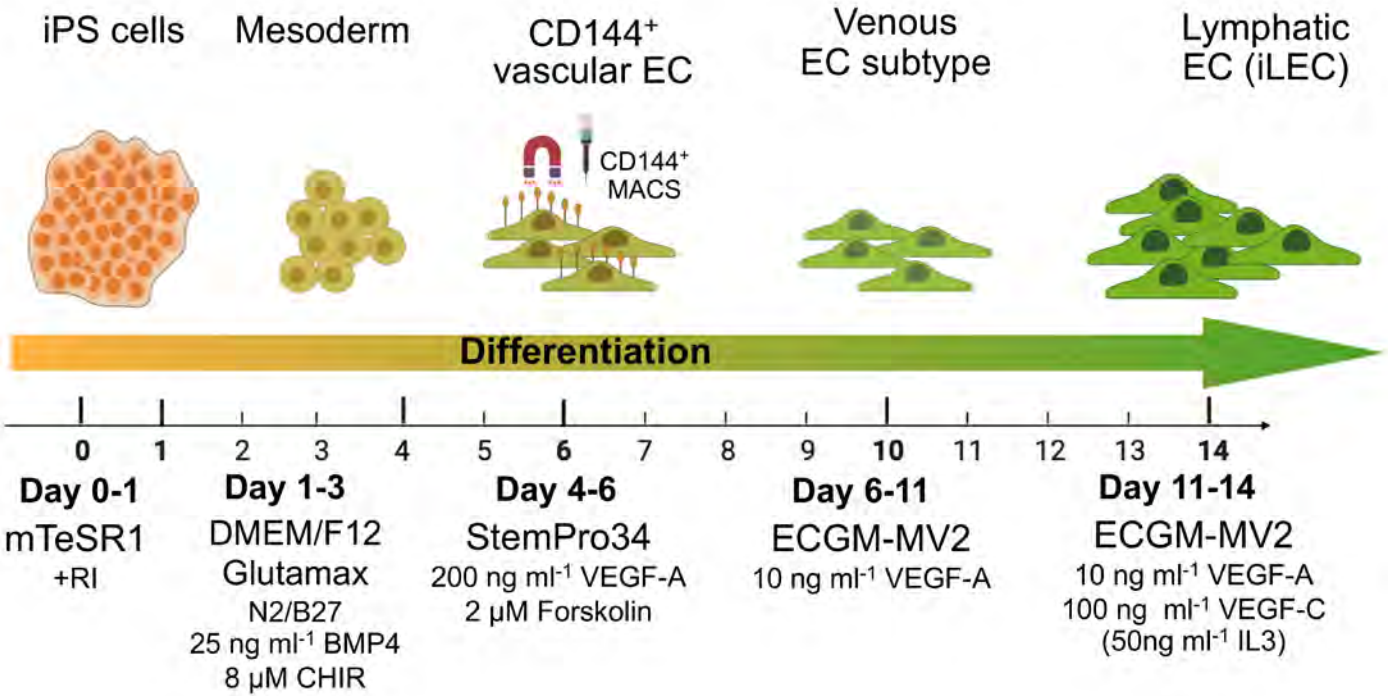
iPS cells
Mesoderm
CD144+ vascular EC
Venous EC subtype
Lymphatic EC (iLEC)
CD144+ MACS
Differentiation
0 1 2 3 4 5 6 7 8 9 10 11 12 13 14
Day 0-1
mTeSR1
+RI
Day 1-3
DMEM/F12
Glutamax
N2/B27
25 ng ml-1 BMP4
8 µM CHIR
Day 4-6
StemPro34
200 ng ml-1 VEGF-A
2 µM Forskolin
Day 6-11
ECGM-MV2
10 ng ml-1 VEGF-A
Day 11-14
ECGM-MV2
10 ng ml-1 VEGF-A
100 ng ml-1 VEGF-C
(50ng ml-1 IL3)

Figure 3

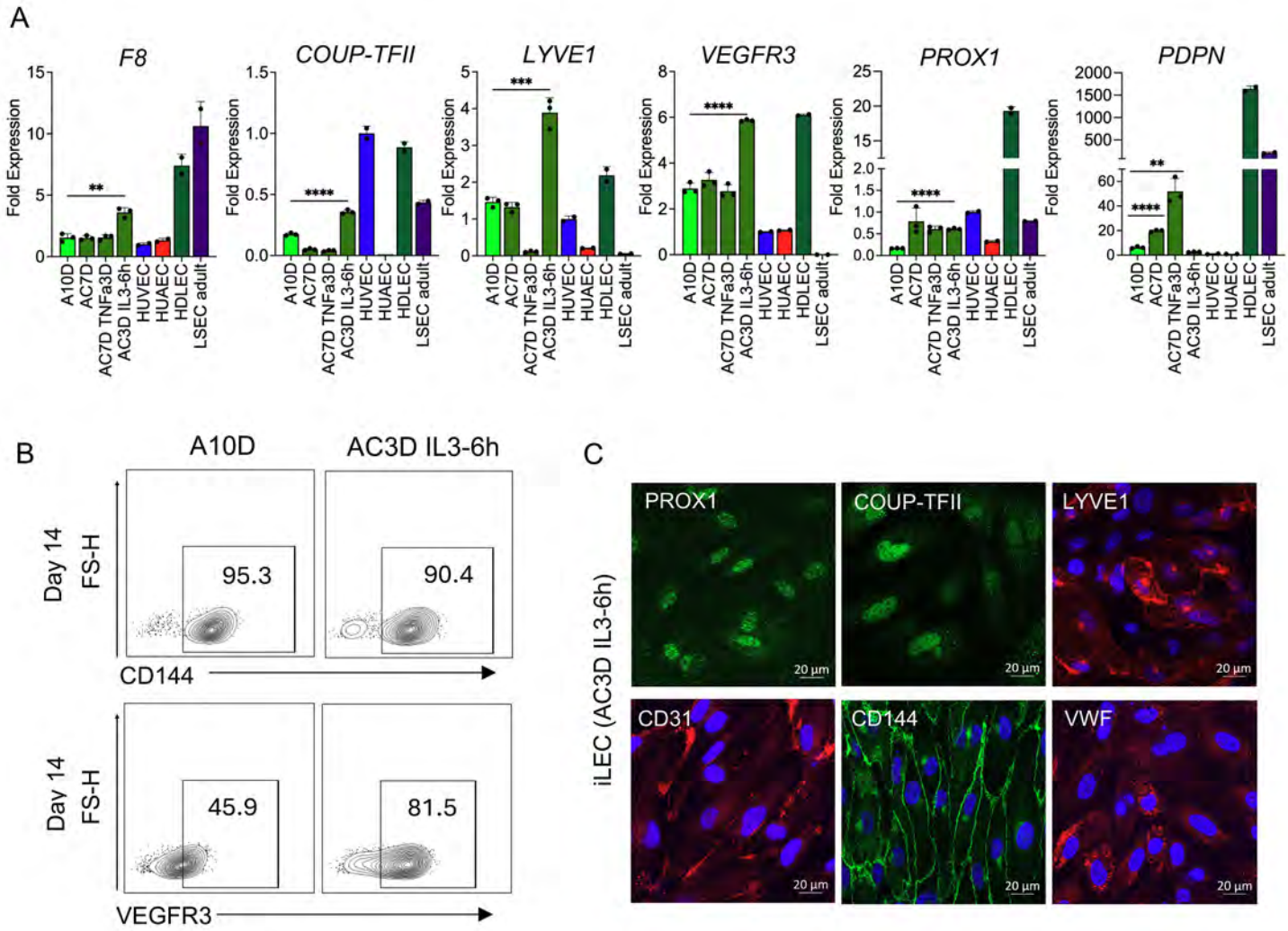
A
F8
COUP-TFII
LYVE1
VEGFR3
PROX1
PDPN
Fold Expression
A10D
AC7D
AC7D TNFa3D
AC3D IL3-6h
HUVEC
HUAEC
HDLEC
LSEC adult
B
A10D
AC3D IL3-6h
Day 14
FS-H
95.3
90.4
CD144
45.9
81.5
VEGFR3
C
iLEC (AC3D IL3-6h)
PROX1
COUP-TFII
LYVE1
CD31
CD144
VWF
20 µm

Figure 4

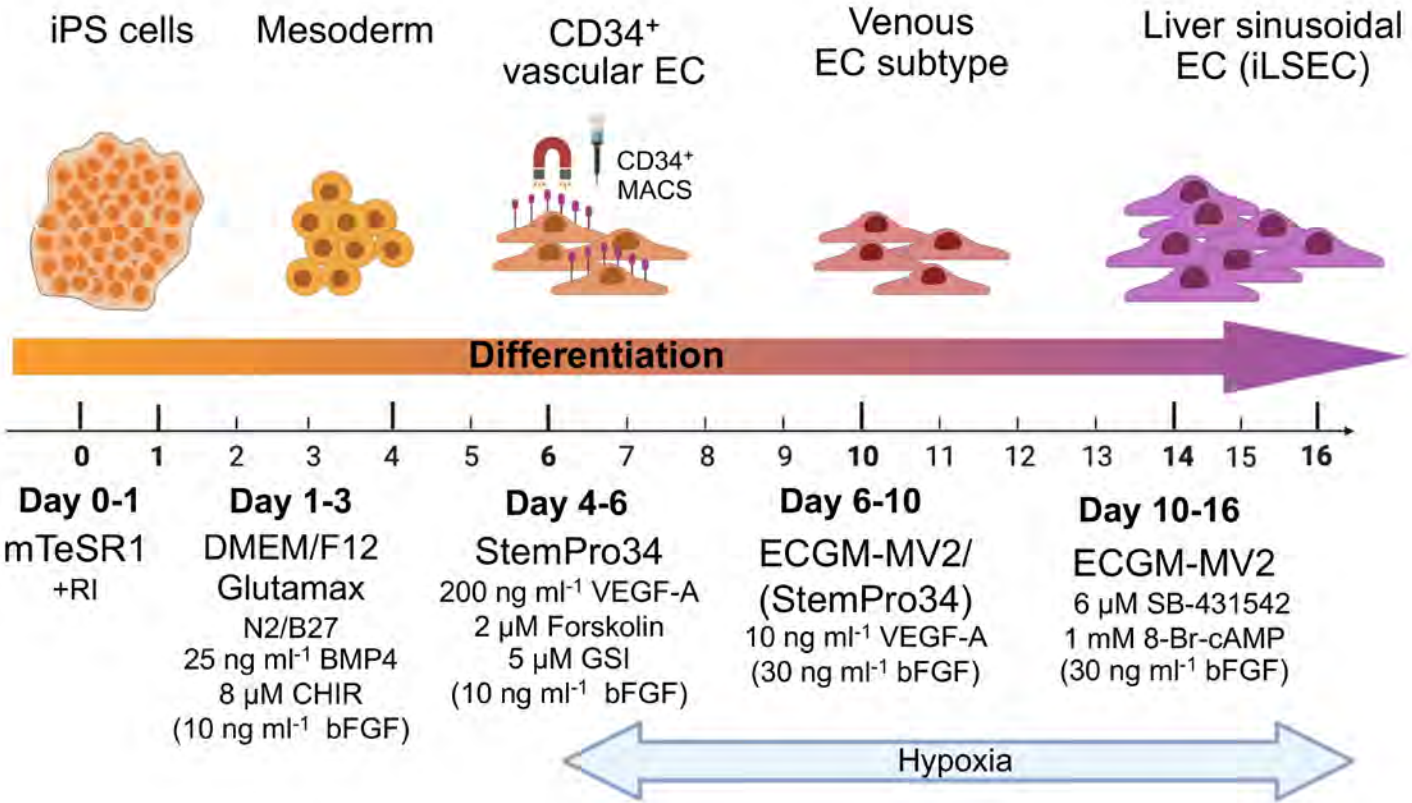
iPS cells
Mesoderm
CD34+ vascular EC
Venous EC subtype
Liver sinusoidal EC (iLSEC)
CD34+ MACS
Differentiation
0 1 2 3 4 5 6 7 8 9 10 11 12 13 14 15 16
Day 0-1
mTeSR1
+RI
Day 1-3
DMEM/F12
Glutamax
N2/B27
25 ng ml-1 BMP4
8 μM CHIR
(10 ng ml-1 bFGF)
Day 4-6
StemPro34
200 ng ml-1 VEGF-A
2 μM Forskolin
5 μM GSI
(10 ng ml-1 bFGF)
Day 6-10
ECGM-MV2/
(StemPro34)
10 ng ml-1 VEGF-A
(30 ng ml-1 bFGF)
Day 10-16
ECGM-MV2
6 μM SB-431542
1 mM 8-Br-cAMP
(30 ng ml-1 bFGF)
Hypoxia

Figure 5

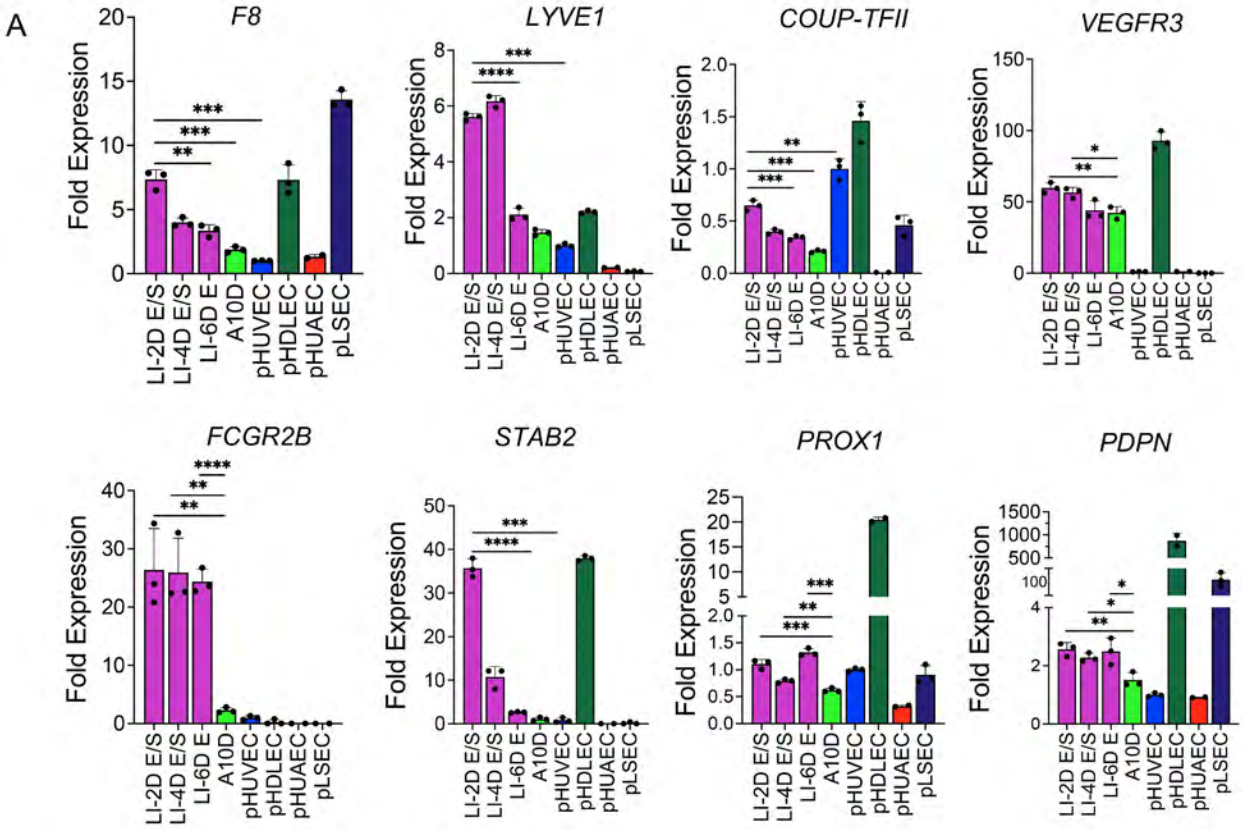
A
F8
LYVE1
COUP-TFII
VEGFR3
FCGR2B
STAB2
PROX1
PDPN
Fold Expression
LI-2D E/S
LI-4D E/S
LI-6D E
A10D
pHUVEC
pHDLEC
pHUAEC
pLSEC

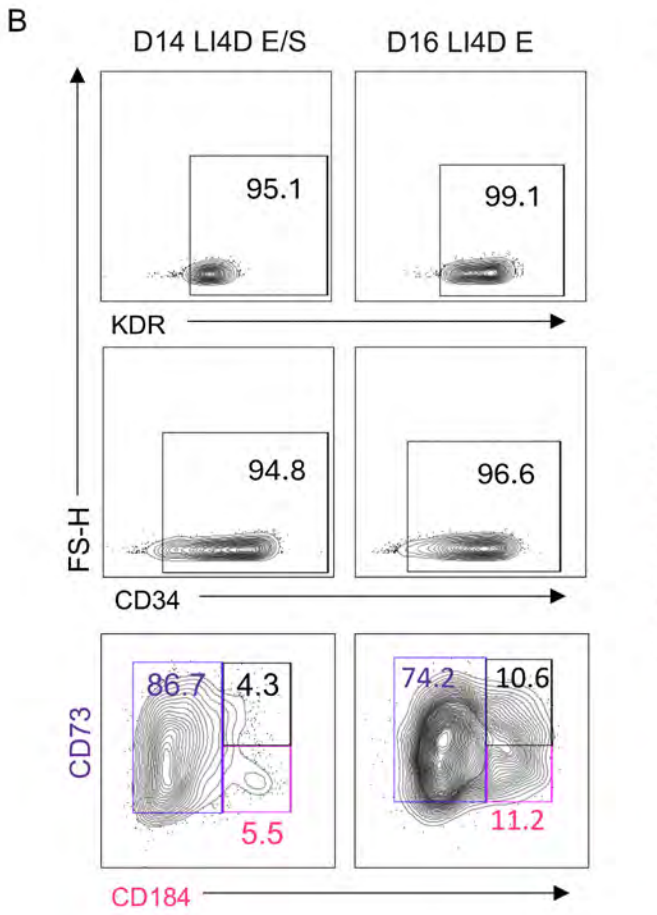
B
D14 LI4D E/S
D16 LI4D E
95.1
99.1
KDR
FS-H
94.8
96.6
CD34
86.7
4.3
5.5
74.2
10.6
11.2
CD73
CD184

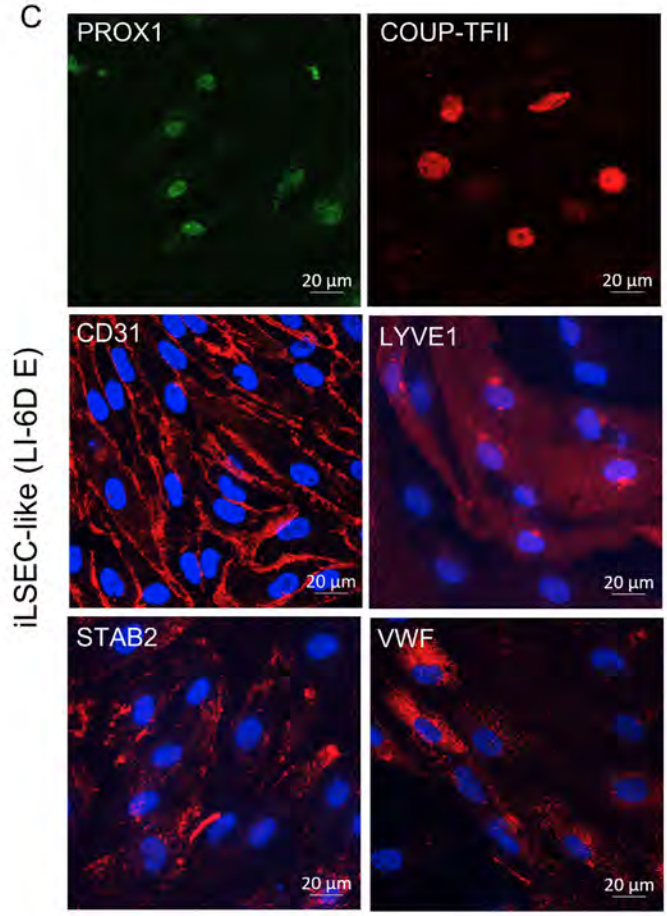
C
iLSEC-like (LI-6D E)
PROX1
COUP-TFII
CD31
LYVE1
STAB2
VWF
20 µm

Figure 6

A

Sample	Peptides found	Domain	Positions
Cm1	DFPILPGEIFK	A2	519-529
	NVILFSVFDENR	A2	591-602
	GELNEHLGLLGPYIR	A3	1769-1783
	VDLLAPMIIHGIK	C1	2092-2104
	SNAWRPQVNNPK	C2	2235-2246
	IHPQSWVHQIALR	C2	2327-2339

B

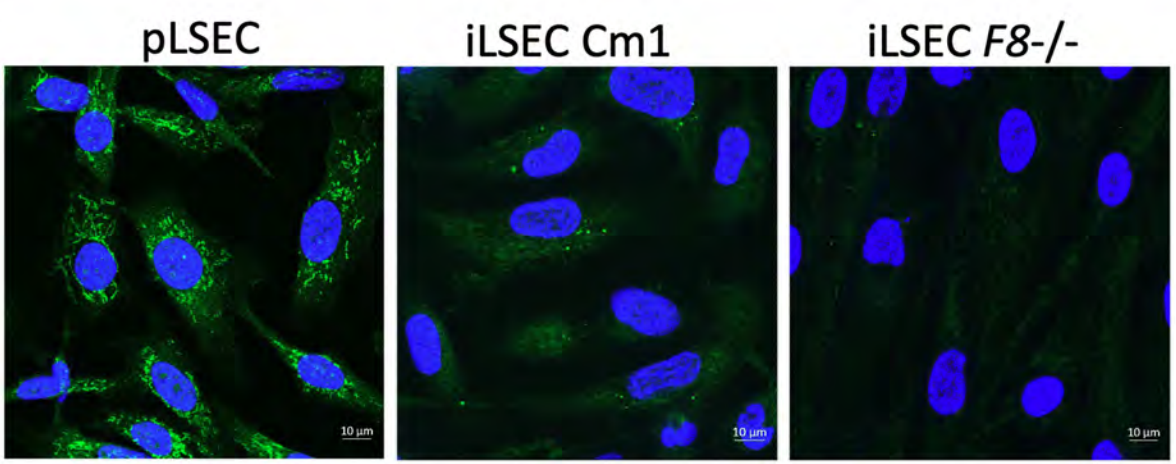

Figure 7

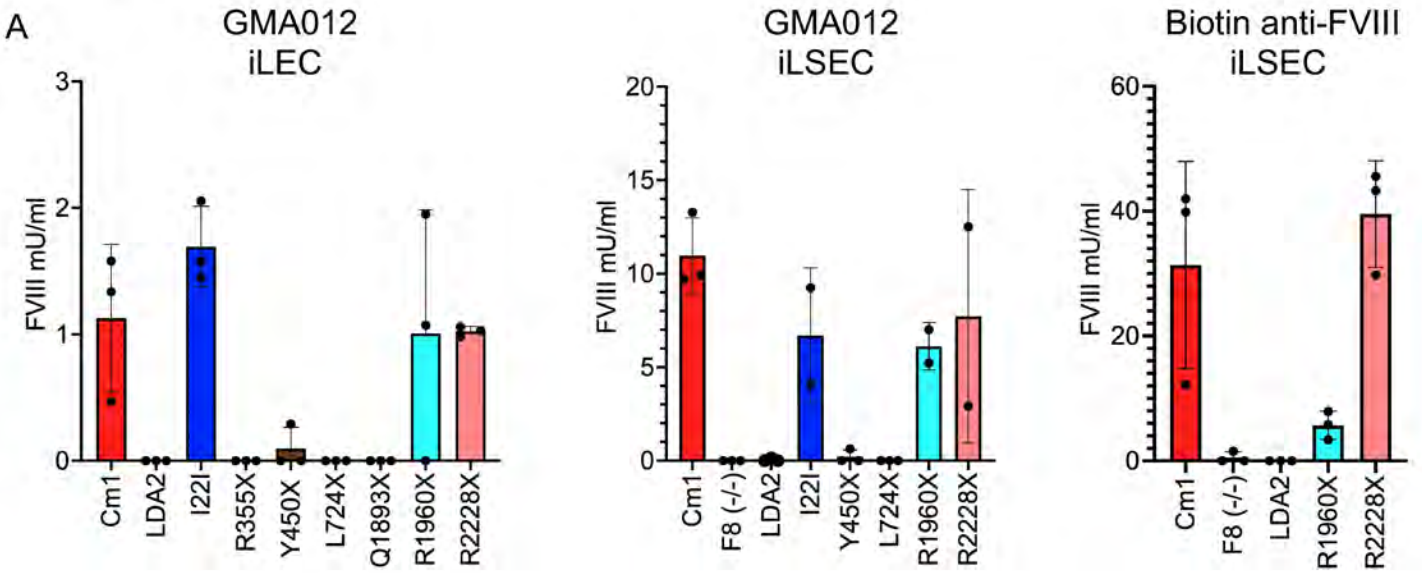
A
GMA012
iLEC
FVIII mU/ml
Cm1
LDA2
I22I
R355X
Y450X
L724X
Q1893X
R1960X
R2228X
GMA012
iLSEC
FVIII mU/ml
Cm1
F8 (-/-)
LDA2
I22I
Y450X
L724X
R1960X
R2228X
Biotin anti-FVIII
iLSEC
FVIII mU/ml
Cm1
F8 (-/-)
LDA2
R1960X
R2228X

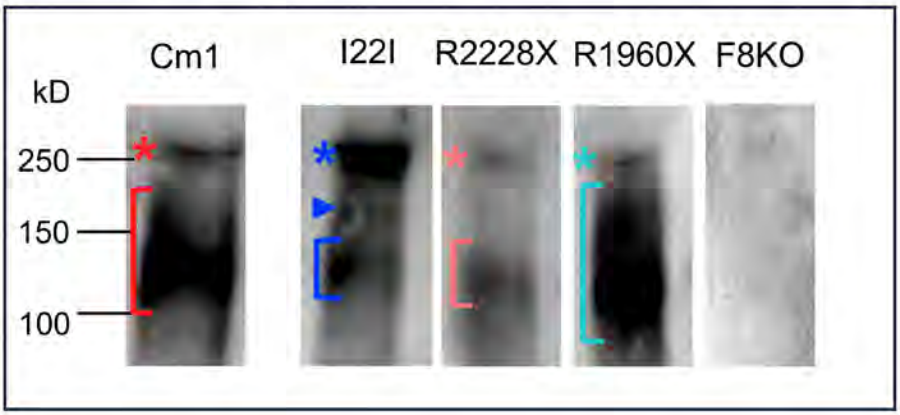
B
IP: SAF8C / WB: GMA012
Cm1
I22I
R2228X
R1960X
F8KO
kD
250
150
100

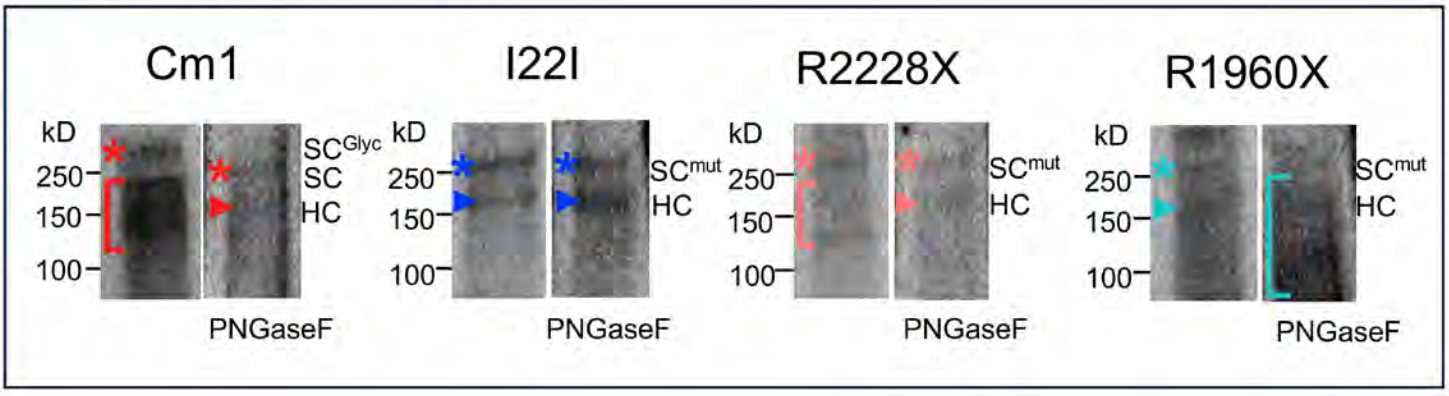
C
IP: GMA012 / WB: SAF8C
Cm1
I22I
R2228X
R1960X
kD
250
150
100
SCGlyc
SC
HC
SCmut
HC
PNGaseF

Figure 8

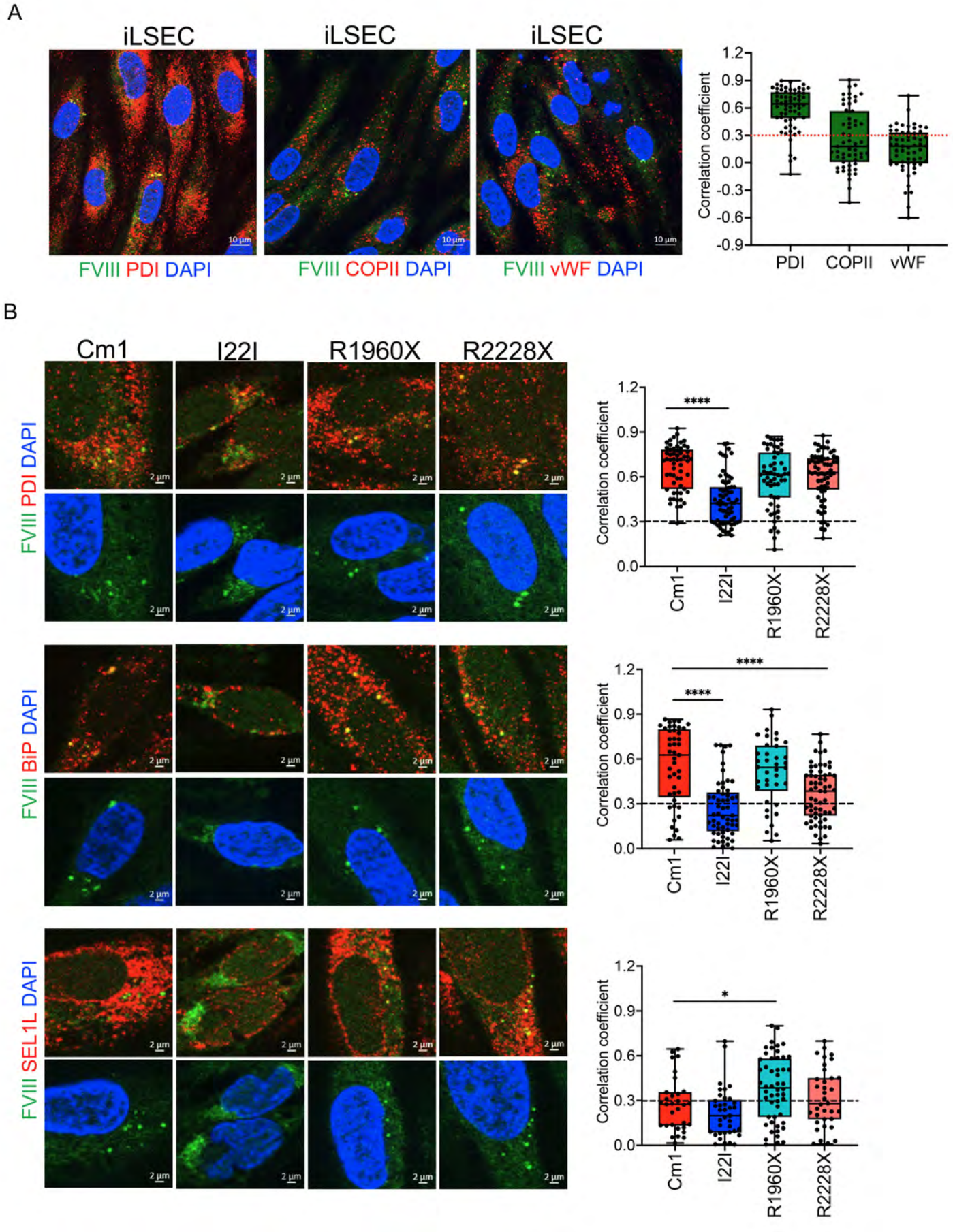
A
iLSEC
iLSEC
iLSEC
10 µm
FVIII PDI DAPI
FVIII COPII DAPI
FVIII vWF DAPI
Correlation coefficient
1.2
0.9
0.6
0.3
0.0
-0.3
-0.6
-0.9
PDI
COPII
vWF
B
Cm1
I22I
R1960X
R2228X
FVIII PDI DAPI
FVIII BiP DAPI
FVIII SEL1L DAPI
2 µm
Correlation coefficient
****
****
****
*
Cm1
I22I
R1960X
R2228X

Supplemental Information

Divergent processing of FVIII light chain variants: secretory potential versus proteasomal retention

Heike Singer,[1,*] Payal Chawla,[1,*] Katrin J. Czogalla-Nitsche,[1] Pujan Engels,[1] Francesco Forin,[1] Marc Sylvester,[2] Melanie Rath,[1] Jens Müller,[1] Tobias Feist,[1] Behnaz Pezeshkpoor,[1] Rawya Al-Rifai,[1] Osman El-Maarri,[1] Johannes Oldenburg,[1,#]

[1]Institute of Experimental Hematology and Transfusion Medicine, University of Bonn, Germany

[2]Medical Faculty, Core Facility Mass Spectrometry, Institute of Biochemistry and Molecular Biology, University of Bonn, Bonn, Germany

#Correspondence: johannes.oldenburg@ukbonn.de

[*]HS and PC contributed equally as co-first authors

EXPERIMENTAL MODEL AND STUDY PARTICIPANT DETAILS

Reprogramming blood from HA-patients

For proof of pluripotency stable iPS cell clones were characterized similarly (Figure S1 & S2). Silencing of the reprogramming transgene was confirmed by endpoint PCR detecting episomal vectors using two sets of primer (oriP and EBNA-1) (Figure S1). Genomic integrity was proven using the microarray PsychArray-24 (Illumina) (Figure S3).

METHOD DETAILS

CRISPR knockout of F8 in iPS wild type

As a negative control for ELISA measurements and immunofluorescent stainings a *F8* iPS knock-out cell line was generated using CRISPR/Cas9 (Figure S4). A custom-made, all-in-one gRNA-Cas9 plasmid with a pRP vector backbone (Vector ID: VB191212-1282zuu) was purchased from VectorBuilder. This vector includes an eGFP sequence to track transfection efficiency, a puromycin resistance cassette for selection, a sequence encoding hCas9 and two gRNAs targeting exon 1 and exon 3 of *F8* (GCCACCAGAAGATACTACCT and TCTGCTAGGTCCTACCATCC). Cm1 wild type iPS cells were transiently transfected with the gRNA-Cas9 plasmid with Lipofectamine Stem Transfection Reagent according to manufacturer's recommendation. 24 hours after transfection cells were selected for two days with 0.3 µg/ml puromycin. After selection, iPS cells were seeded at a concentration of 0.5 cells/well in Matrigel-coated 96-well plates to obtain single cells for clonal expansion. iPS cells were cultured in mTeSR supplemented with 10 µM ROCK inhibitor during transfection, selection and the first three days of clonal expansion. Single cell clones were analyzed by Sanger Sequencing to verify the disruption of *F8* reading frame by INDEL formation following Cas9 DNA cleavage. The following primers were used for both *F8* exon 1 and exon 3 amplification and Sanger Sequencing: *F8* ex1-F (CCCTCCTGGGAGCTAAAGAT), *F8* ex1-R (CACCTTCCTCCAAGCAGACT), *F8* ex3-F (GCTTCTCCACTGTGACCTTGA), *F8* ex3-R (TGACAGGACAATAGGAGGGTATTT).

Differentiation of iPS cells into vascular ECs

Briefly, after generating a single cell suspension of iPS cells, 5,3 x 10^4/cm^2 cells were re-seeded on matrigel in mTeSR1 containing rock inhibitor Y-27632 (final conc 10 µM). Cells were maintained in mesoderm priming medium (MPM) containing DMEM/F12 supplemented with N2 (10 µl/mL), B27 (20 µl/mL), BMP4 (Bone morphogenetic protein-4) (25 ng/mL) and CHIR99021 (Laduviglusib) (8 µM). On day 3, medium was changed. At days 4 to 6, vascular endothelial cell progenitors were induced by maintaining cells in vEC induction medium containing StemPro™-34 supplemented with VEGF-A (200 ng/mL), forskolin (2 µM) and

penicillin/streptomycin (1%). On day 6, cells were detached using Accutase, collected, and centrifuged. Single-cell suspensions were subjected to magnetic activated cell sorting (MACS) for positive selection of CD144 vascular EC (vEC) or CD34 angioblasts according to the manufacturer's instructions.

Differentiation of iPS into iLEC and iLSEC

Day 6 angioblasts for both subtypes were seeded at a cell density of 5,2x10x^4 cells/cm^2 on tissue culture plates coated with fibronectin.

Characterization and functional assays of MACS-isolated vECs

For proof of angiogenic potential, 7x10^4 MACS-isolated vECs were seeded on a 24-well plate coated with 300 µl growth-reduced factor Matrigel^{TM} (Corning) in ECGM-MV2 medium (PromoCell). The ability to form tubular structures was investigated periodically after 2, 4, 6 and 8 hours on a light microscope (Zeiss) (Figures S1C & S2C). For lipid uptake assay, 3x10^4 day 8 vEC's were seeded as biological triplicates in a 96-well plate with ECGM-MV2 medium. After 48 hours medium was supplemented with LDL-DyLight^{TM} 550 (Abcam) (1:100). After 5 hours, degree of LDL uptake was examined under a fluorescent microscope (Axio Observer.7 with ApoTome.2, Zeiss) (Figures. S1C & S2C). Differentiation efficiency between day 0 to 6 was monitored by rt-qPCR (Figure S5).

Specification analysis towards iLEC upon CD144$^+$ MACS separation

For specification analysis marker expression from primary pHUVEC, pHUAEC, pHDLEC and pLSEC was conducted to normalise common, venous, arterial, LEC and LSEC marker to pHUVEC (Figure S6). Starting day 6 CD144+ vECs were cultured in ECGM-MV2 supplemented with low levels of VEGF-A (10 ng/ml). RNAs collected on day 10, 15 and 23 were normalised to pHUAEC for venous marker expression and normalised to HUVEC for arterial and F8 expression (Figure S7). For iLEC specification Trial 1 (T1), vEC were supplemented with VEGF-A (10 ng) and VEGF-C (100 ng) and collected RNAs from day 13, 16 and 21 were analysed for lymphatic marker expression and normalised to pHDLEC. For iLEC specification Trial 2 (T2), vEC were supplemented with VEGF-A (10 ng), VEGF-C (100 ng) and Angiopoietin-1 (20 ng). Collected RNAs from day 10, 16 and 23 were analysed as in T1.

Inflammatory Cytokine Stimulation

Starting day 6 CD144$^+$ vECs were cultured in ECGM-MV2 supplemented with low levels of VEGF-A (10 ng/ml) until day 9. On day 9, the cells were treated with various cytokines for 6 hours (Figure S8). The cytokine treatments included IL-6, IL-3, TNF-α, IL-1β and IFN-γ at concentrations of either 50 ng/ml or 100 ng/ml. Finally in a biological triplicate experiment, cells

were treated with IL-3, TNF-α or IL-6 at concentrations of 20 ng/ml or 50 ng/ml. In control treatments, medium only supplemented with bovine serum albumin (BSA) at concentrations corresponding to those used in cytokine dilutions was added to the cells.

RNA analyses

Total RNA from day 6 $CD144^+$ vEC was isolated using the PureLink™ RNA mini kit, according to the manufacturer's instructions. The concentration and purity of RNA was determined using a ND-1000 spectrophotometer (Nanodrop). cDNA was synthesized using the QuantiNova™ Reverse Transcription Kit. Overlapping rt-PCR was performed according to the published protocol. [59] For specification analyses of the iLEC and iLSEC model, cells were harvested between day 12 to 16 and RNA extractions were prepared using the PureLink™ RNA mini kit, according to the manufacturer's instructions. RT-qPCR for iPS, mesoderm, common EC, venous, arterial, lymphatic and LSEC marker was implemented using the AgPath-ID™-Kit with appropriate primer-probe pair (Table S1).

Following cytokine treatment, day 10 $CD144^+$ vEC were isolated as above and subjected to rt-PCR analysis.

ELISA

GMA012: Plates were coated with the antibody (5 µg/ml) over night. After washing thrice (1x PBS, 0.05% Tween, 3 mM $MgCl_2$) and blocking for two hours with 2% BSA, triplicates from each sample (1:6 dilution) was incubated for four hours at room temperature. Next, wells were washed thrice and further incubated with detection antibody SAF8C-HRP (2 µg/ml). Finally, upon washing, chemiluminescence ELISA substrate was added and luminescence was measured by multi-detection microplate reader (Synergy2, Biotek). Standard curve was prepared using HEK *F8*$^{-/-}$ cellular lysate diluted in NP40 lysis buffer (1:6) adding different concentrations (5, 7.5, 10, 20, 40, 80, 160, 320 mU) of recombinant full-length FVIII (Kogenate). EC specific lysates from Cm1 and I22I were defined as positive controls, whereas EC lysates LDA2 and Cm1 *F8*$^{-/-}$ were used as negative controls.

CaptureSelect™ biotin anti-FVIII conjugate: Wells were coated with streptavidin (1 µg/mL) and incubated overnight. The following day, the plate was washed with washing buffer (1x PBS, 0,05% Tween, 0,1% BSA). Wells were coated with the antibody (2 µg/mL) and incubated for 2 hours at RT. After another washing step, samples were added at a 1:12 dilution with 1xPBS supplemented with 0,1% Tween and 0,1% BSA and incubated for 2 hours at RT. Detection antibody SAF8C-HRP (2 µg/mL) was added and incubated for 1 hour at room temperature post another washing step. After a final wash, the chemiluminescent ELISA substrate was added, and luminescence was measured in the microplate reader using the above-mentioned standard curve (1:12).

FACS analyses

Cells on day 0, 4, 6, 10, 12 and 14 were detached using Accutase collected, centrifuged and stained with primary antibodies according to the manufacturer's instructions 10 minutes at 4°C in FACS buffer (PBS+0.2 mM EDTA+0.5% BSA). Upon incubation, cells were washed and resuspended in FACS buffer for analysis using Beckman Coulter Life sciences, Navios EX flow cytometry platform. Data analysis was further conducted on FlowJo v10.9. Gating based on FMO controls (Figure S9). To evaluate the inflammatory responsiveness and antigen-presenting potential of the differentiated endothelial cells, iPSC-derived vascular endothelial cells (vEC) were stimulated at day 13 of differentiation with 50 ng/ml or 100 ng/ml IFN-γ for 6 h or 24 h (S10-A). Total RNA was isolated and analysed by real-time PCR for *PD-L1* and *PD-L2* expression. In parallel, primary HUVEC, primary HDLEC and iPSC-derived vEC (A10D) were treated with 100 ng/ml IFN-γ for 24 h to determine *CIITA* induction as a transcriptional activator of MHC-II (S10-B). For flow cytometry, iPSC-derived vEC (A10D) and iLSEC (LI-4D E/S) were stimulated with 100 ng/ml IFN-γ for 24 h and stained for MHC-I using REA230 (HLA-A, B, C) and MHC-II using antibody WR18 (HLA-DR, -DQ, -DP). Both endothelial subtypes showed a clear upregulation of MHC-I, while MHC-II was also increased with slightly lower intensity in iLSEC (S10-C).

Immunofluorescence (IF)

Differentiated iLSECs were cultured on 12-well cover slips until day 14. After fixation with 4% paraformaldehyde (RT/10 minutes), cells were blocked with PBS containing 0.1 M Glycine, 1% BSA and 0,1% Saponin for 1 hour at RT. Cells were incubated at 4°C overnight with primary antibodies diluted in PBS containing 1% BSA and 0,1% saponin. Cells were washed with the blocking medium and incubated at RT for 60 minutes with the corresponding secondary antibodies (Table S1).

When stained with biotin anti-FVIII conjugate, cells were additionally blocked with Ready Probes™ Streptavidin/Biotin blocking solution according to the manufacturer´s instructions to avoid cross-reaction with endogenous biotin. Finally, cells were incubated overnight with biotin anti-FVIII conjugate and visualized with Streptavidin Alexa488.

Western Blot

For a second approach, lysates from $10x10^6$ iLSEC were subjected to immunoprecipitation using the monoclonal anti-A2 antibody GMA012. The eluates were then split: one half was directly loaded onto SDS-PAGE and probed by Western blot using SAF8C-AP; the other half underwent PNGase F treatment (New England Biolabs, #P0704S) to assess glycosylation status. Briefly, eluates were denatured in glycoprotein denaturation buffer (10 min, 99 °C), then incubated with PNGase F (1 h, 37 °C) in the presence of GlycoBuffer 2 and NP-40. Following

digestion, samples were mixed with Laemmli buffer (1:1 with BME), heated at 95 °C for 5 min, and loaded on 7,5% TGX gel.

Chromatography parameters and mass spectrometry conditions

Peptide separation was performed on a Dionex Ultimate 3000 RSLC nano HPLC system coupled to an Orbitrap Fusion Lumos mass spectrometer. Dried peptides were dissolved in 10 µl 0.1% formic acid (solvent A) and 15% were injected onto a C18 analytical column (400 mm x100 µm, 3 µm). For targeted analysis, peptides were separated as above (90 min gradient). 24 Coagulation factor VIII peptides across all processed regions were chosen based on the unique SRM peptides in the nextprot database (www.nextprot.org) and manual curation. Precursors with z=2 and / or z=3 were chosen for isolation and fragmentation. MS1 spectra were acquired from 330 to 1200 m/z in the Orbitrap every 3 seconds with a maximum inject time of 50ms (R=60,000, gain control target 400,000). Target ions were subjected to stepped-HCD fragmentation (1.0 Da quadrupole isolation, collision energy 28%) and product ions analysed in the Orbitrap with a maximum inject time of 32 ms (R=15,000, gain control=50,000).

Data analysis

Peptide identification was done with an in-house Mascot server version 2.8.1 against human sequences of SwissProt (2022_02, 20,387 human sequences) and a collection of common contaminants. Precursor ion *m/z* tolerance was 10 ppm, fragment ion tolerance 20 ppm. Tryptic peptides were searched for up to two missed cleavages. Propionamide was set as a static modification of cysteines, while oxidation of methionine and acetylation of protein N-termini were set as dynamic modifications. Spectrum confidence of Mascot results was assessed by the Percolator algorithm 3.05 as implemented in Proteome Discoverer software 2.5.0.400.[60] Spectra without high confident matches (q-value > 0.01) were sent to a second round Mascot search with semi-specific enzyme cleavage and changing the modification of cysteines with propionamide to dynamic. Database search results were maintained at a 1% false discovery rate for reliable protein identifications. Validation of MS2 spectra was aided by a spectral library created on the PROSIT server.[62] Quantification was done on MS2 level.

Quantification and Statistical Analysis

Graph Pad Prism was used to plot heatmap an rt-PCR results. *t*-test was performed between two analyses with $p<0.05$ deemed significant.

IEDB Analysis of MHC-I and MHC-II Binding and Processing

HLA class I (A, B, C) and class II (HLA-DR, DP, DQ) genotyping of the patients was performed using the AllType™ FASTplex™ NGS Assay kits (One Lambda, A Thermo Fisher Scientific)

according to the manufacturer's instructions. DNA sequencing library was sequenced on a MiniSeq DNA sequencer (Illumina Inc., SanDiego, CA). Data analysis was performed using the TypeStream Visual software (One Lambda).

In silico predictions of FVIII-derived peptide presentation were performed using the Immune Epitope Database (IEDB). FVIII wild-type and patient-specific truncated sequences were analyzed. I22I in silico transcript ends after exon 22 (at AA 2143), followed by translation into intron 22 until the first stop codon appears. This yields a truncated peptide ending with three extra amino acids: V, C, N (from GTA, TGT, AAT).

For MHC-I, NetMHCpan 4.1 (EL and BA models) together with the IEDB processing module (proteasome cleavage, TAP transport, binding) and the immunogenicity tool were applied. For MHC-II, NetMHCIIpan 4.1 EL, the CD4 Epitope Score, and the MHC-II NP module were used. Predictions were filtered for strong binders and peptides with high predicted immunogenicity, and results were reported as exploratory analyses (Figures S13–14).

Figures: Created in BioRender. Singh, S. (2025) https://BioRender.com/undefined

Supplemental Figures and Tables:

Figure S1: Functional characterization of iPS and A10D vEC for wild type Cm1 and two HA patient samples I22I and LDA2.

A. Stable iPS cells were characterized by staining with specific pluripotency marker AP Live, Nanog, SSEA-4, Tra-1-60, and Oct-4. B. iPS cell derived embryoid bodies tested for spontaneous differentiation into all three germ layers by immunofluorescent staining (IF) using antibodies against actin smooth muscle (ASM), ß-Tubulin III and α-feto protein. C. Tube forming assay presents the angiogenic potential of CD144 MACS isolated vEC maintained 10 Days in 10ng VEGF-A = A10D (left picture cluster). LDL-uptake assay visualized uptake of LDL-DyLight™ 550 (red signal) in all three samples. D. Transgene silencing was confirmed by PCR specific to episomal vectors. E. Mycoplasma negative PCR in all iPS cell derived patient samples. Immunostaining results depicted as a representative image of biological duplicates.

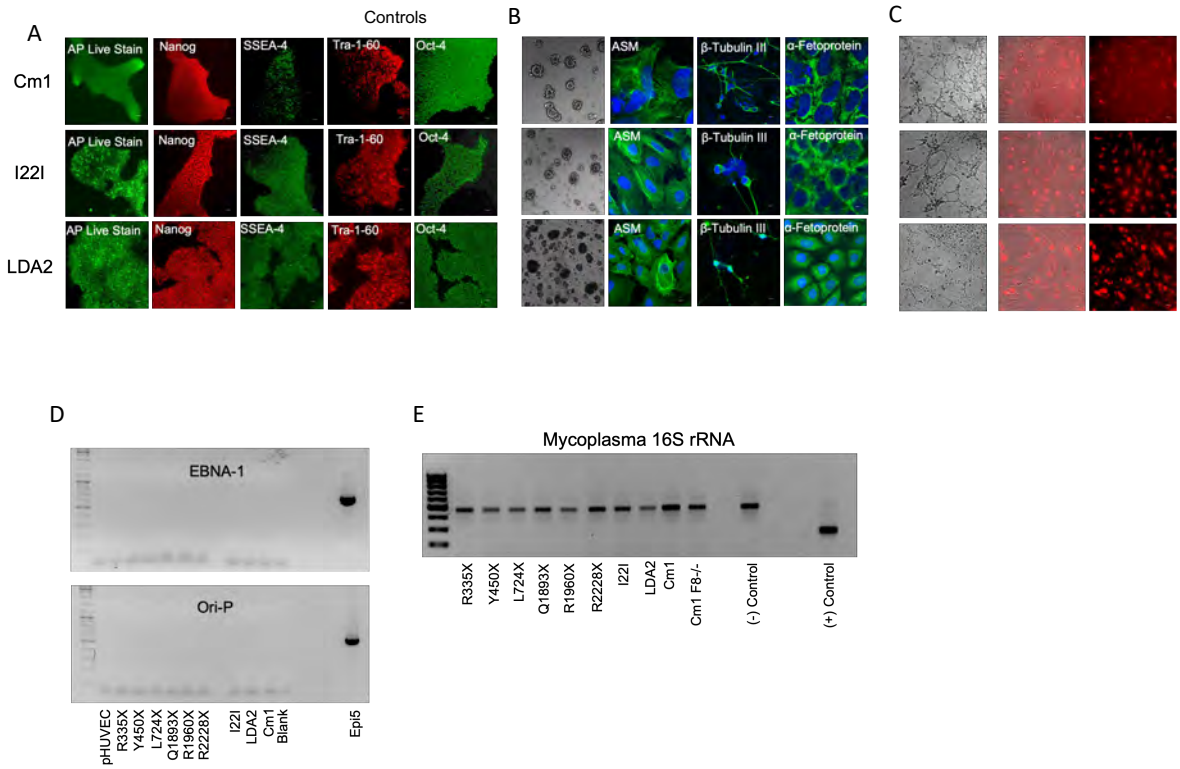

Figure S2: Functional characterization of iPS and A10D vEC for six patient samples with nonsense mutations in the heavy and light chain of FVIII. A. Stable iPS cells were characterized by staining with specific pluripotency marker AP Live, Nanog, SSEA-4, Tra-1-60, and Oct-4.

B. iPS cell derived embryoid bodies tested for spontaneous differentiation into all three germ layers by immunofluorescent staining (IF) using antibodies against actin smooth muscle, β-Tubulin III and alpha-feto protein. C. Tube forming assay presents the angiogenic potential of A10D vEC (left picture cluster). LDL-uptake assay visualized uptake of LDL-DyLight™ 550 (red signal) in all six samples. Immunostaining results depicted as a representative image of biological duplicates.

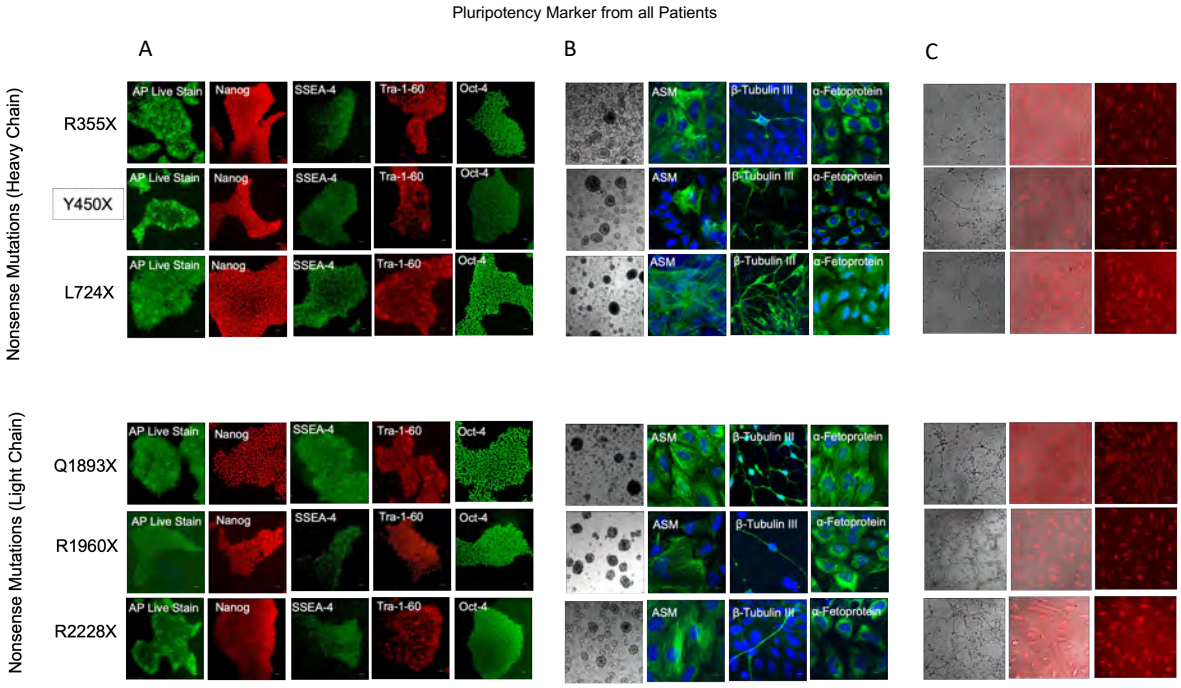

Figure S3: Karyotype analysis.

DNA of stable iPS cell clones from healthy and patients with mutations was analysed using a SNP (single nucleotide polymorphism) array. For each chromosome the B allele frequency (upper blue dotted row) and the log A ratio (lower blue dotted line) was evaluated.

A. Controls: Cm1, Cm1 *F8-/-*, I22I and LDA2

B. Nonsense mutations in the heavy chain: R355X, Y450X, L724X.

C. Nonsense mutations in the light chain: Q1893X, R1960X, R2228X

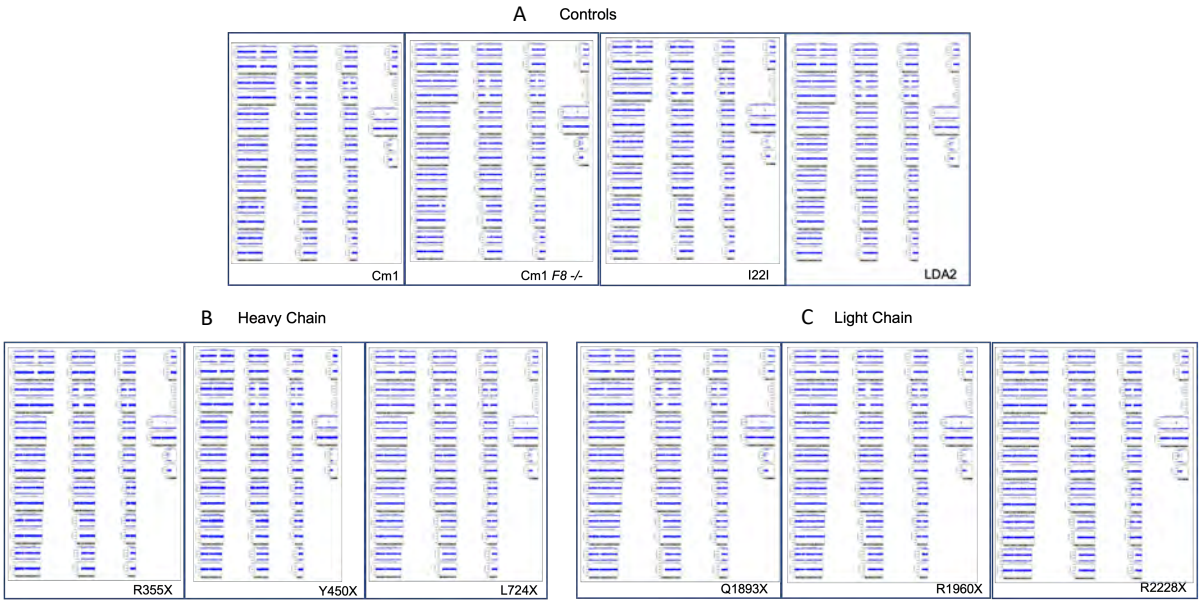

Figure S4: CRISPR-Cas9 mediated knock-out of *F8* gene by targeting exons 1 and 3. The vector map on the left displays two guide RNAs (gRNAs) aimed to target ex1 (green) and ex3 (pink). On the right, sequencing results for IPS clone #31 confirm successful gene disruption. The gRNAs induced a one base pair deletion in exons 1 and 3, causing a frameshift and introducing several premature stop codons.

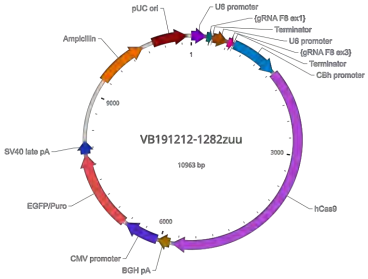

CRISPR vector targeting Ex1&3

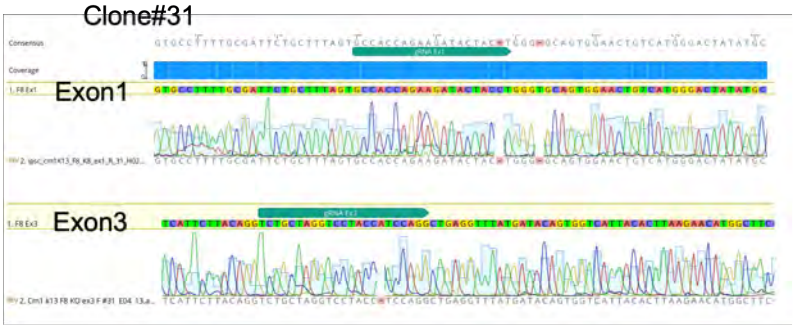

Figure S5: Differentiation efficiency monitored by relative gene expression. On day 0, pluripotency markers *Nanog* and *Sox2* (orange bars) show the highest expression when normalized to β-actin. On day 4, mesodermal marker *Brachyury* (olive bars) shows the highest expression when normalized to β-actin. On day 6, after CD144 MACS isolation endothelial cell marker *CD31* and *CD34* show exclusive expression when normalized to β-actin (light green bars).

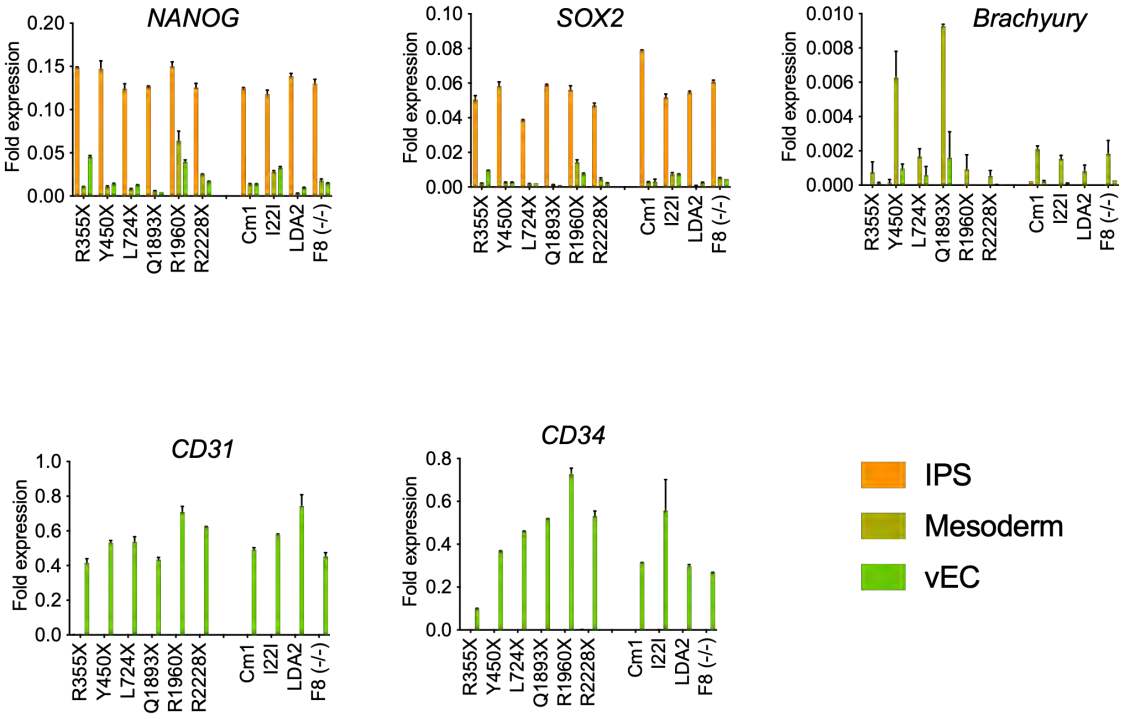

Figure S6: rt-PCR studies for specification of primary human cell lines.

Controls: HUVEC: human umbilical vein endothelial cell, HUAEC: human umbilical arterial endothelial cell, HDLEC: human dermal lymphatic endothelial cell, LSEC: liver sinusoidal endothelial cell. Result denoted as a fold expression to pHUVEC.

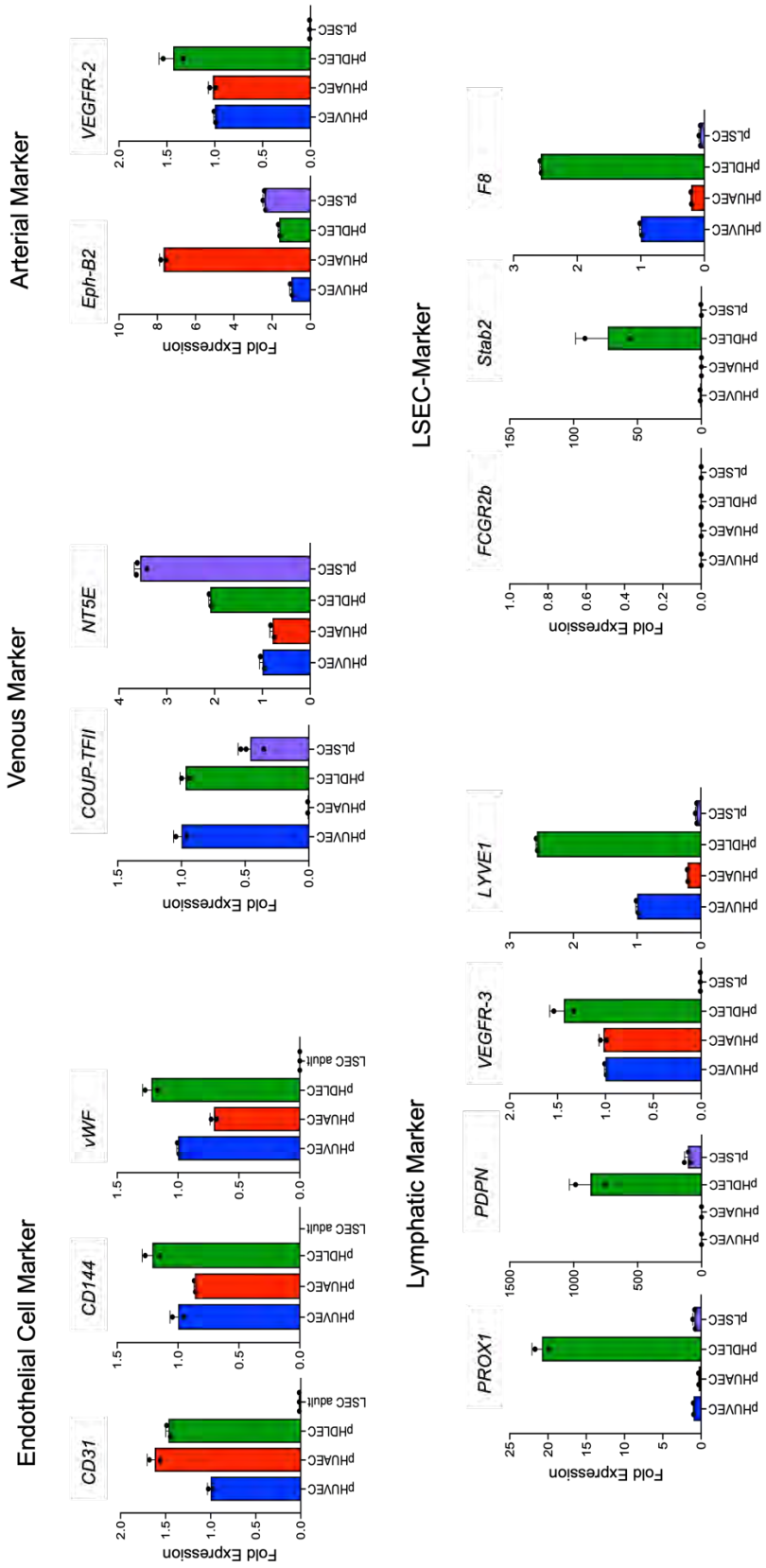

Figure S7: Specification analysis towards iLEC upon CD144$^+$ MACS selection.

A. 10 ng VEGF-A: Venous endothelial progenitors were maintained in 10 ng VEGF-A starting day 6. RNA was collected on day 10, 15 and 23.

B. T1: Venous endothelial progenitors were maintained in a combination of 10 ng VEGF-A and 100 ng VEGF-C. RNA was collected on day 13, 16 and 21.

C. T2: Venous endothelial progenitors were maintained in a combination of 10 ng VEGF-A, 50 ng VEGF-C and 20 ng Angiopoietin-1. RNA was collected on day 10,16 and 23.

Controls: HUVEC: human umbilical vein endothelial cell, HUAEC: human umbilical arterial endothelial cell, HDLEC: human dermal lymphatic endothelial cell, HCMEC: human cardiac microvascular endothelial cell. Result denoted as a fold expression to pHUAEC for venous marker, pHUVEC for arterial marker and *F8,* pHDLEC for lymphatic marker.

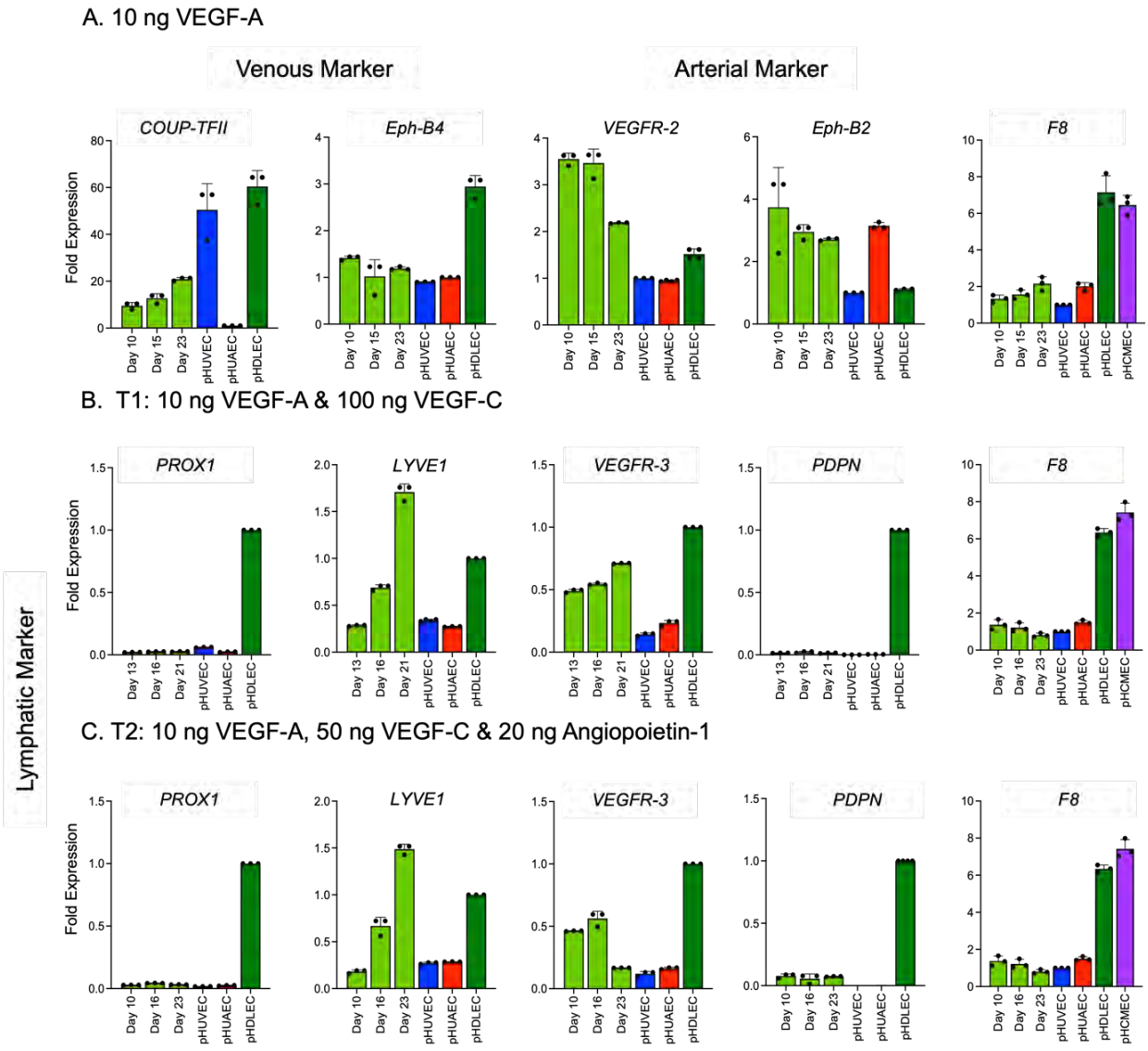

Figure S8: rt-PCR studies to determine inflammatory cytokine influence in vECs and their impact on *F8*.

Cells were treated with 50 ng or 100 ng concentrations of IL-6, IL-3, TNFα, IL-1β and IFN-ɣ for 6 hours and collected as RNA. Grey bars denote untreated cells as control. ***:p<0.001, ****:p<0.0001. Result denoted as fold expression to untreated cells.

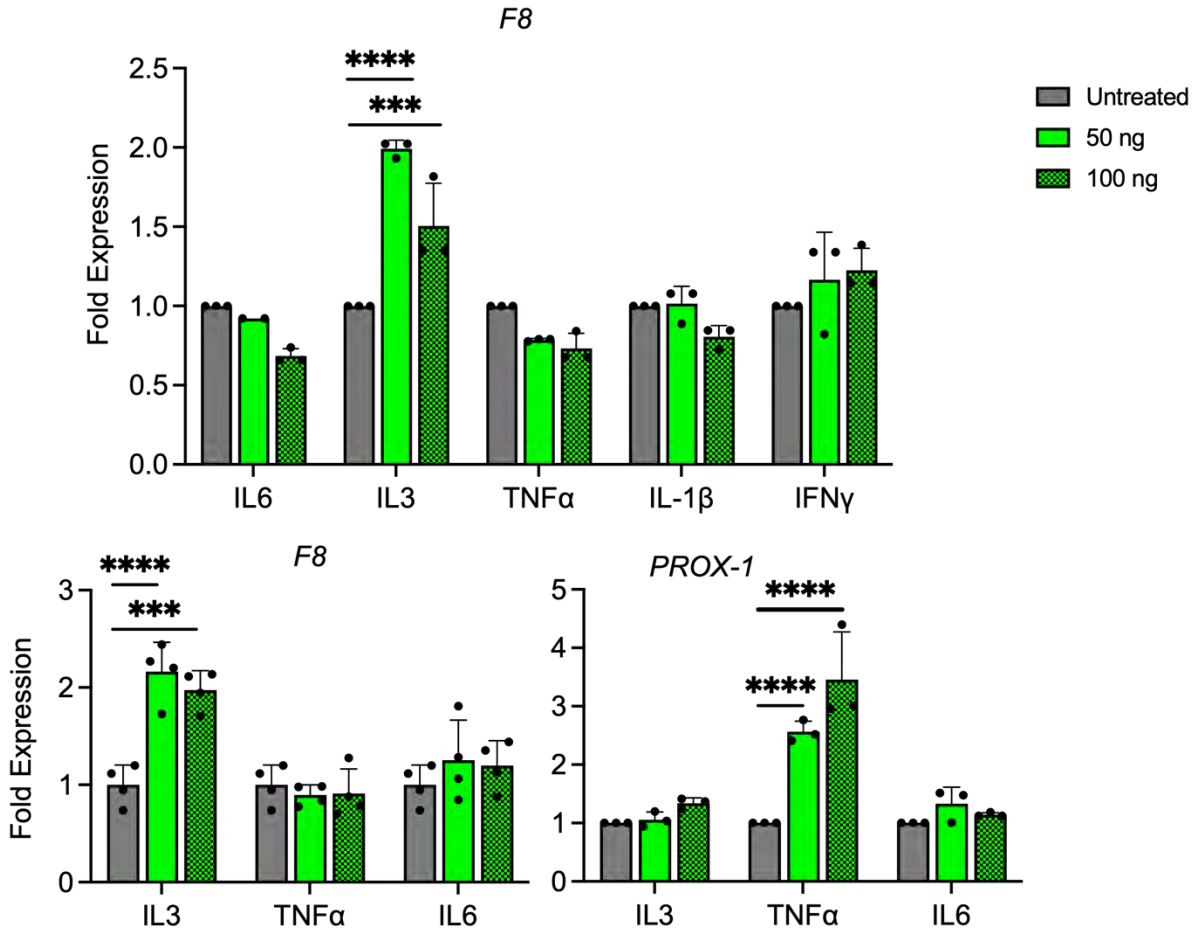

Figure S9: Gating strategy for FACS analysis based on FMO controls. A. A cells gate is created based on FS-A vs SS-A. B. Doublets are removed with a FS-A vs FS-W gate (single cell gate). C. Live cells are selected using a PI as a marker. D. Based on the FMO control of CD34, selection of the CD34+ population was made. E. Similarly using FMO control for CD73 and CD184, selection of a subset of CD34+ cells and subsequent arterial and venous population was selected.

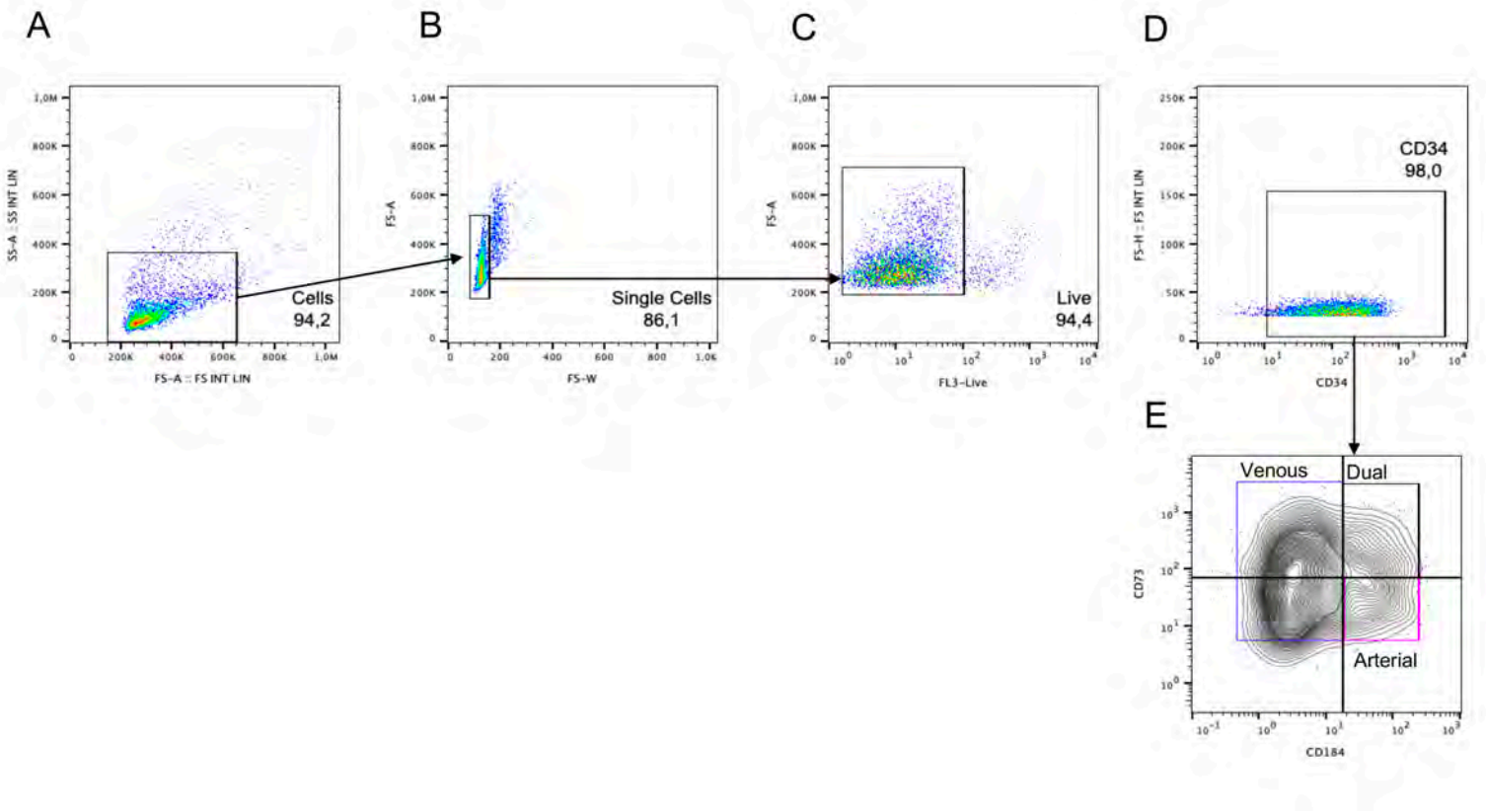

Figure S10. IFNγ–induced immune activation in iPS differentiated endothelial cells.

qPCR and flow cytometry analyses showing induction of *PD-L1*, *PD-L2* and *CIITA* expression as well as upregulation of MHC-I and MHC-II surface molecules in iPSC-derived endothelial cells after IFN-γ stimulation of vEC (A10D) and iLSEC (LI-4D E/S).

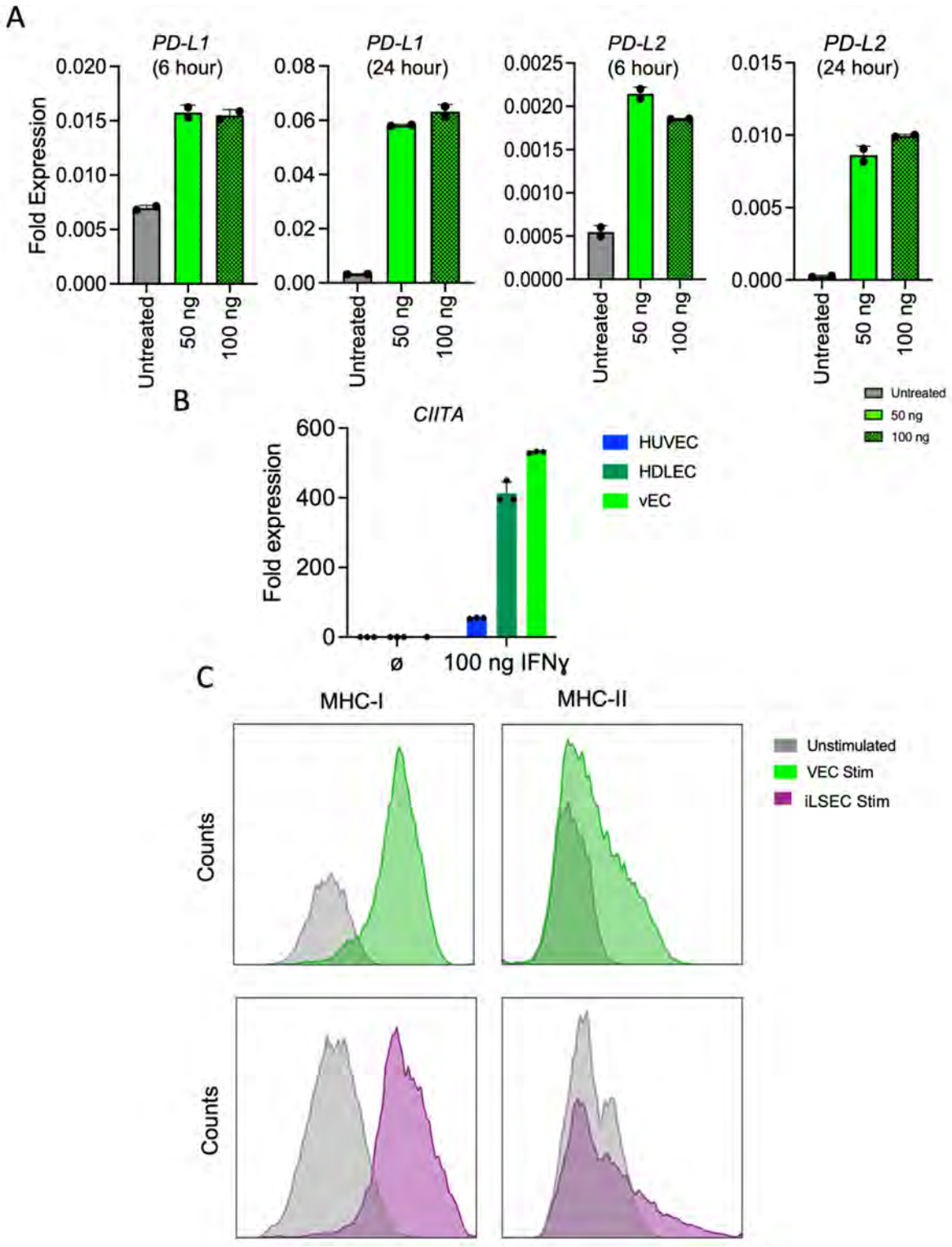

Figure S11: Overlapping semiquantitative rt-PCR representing molecular *F8* mRNA content from vEC differentiated HA-patients (first lane) compared to wild type donor Cm1 (second lane).

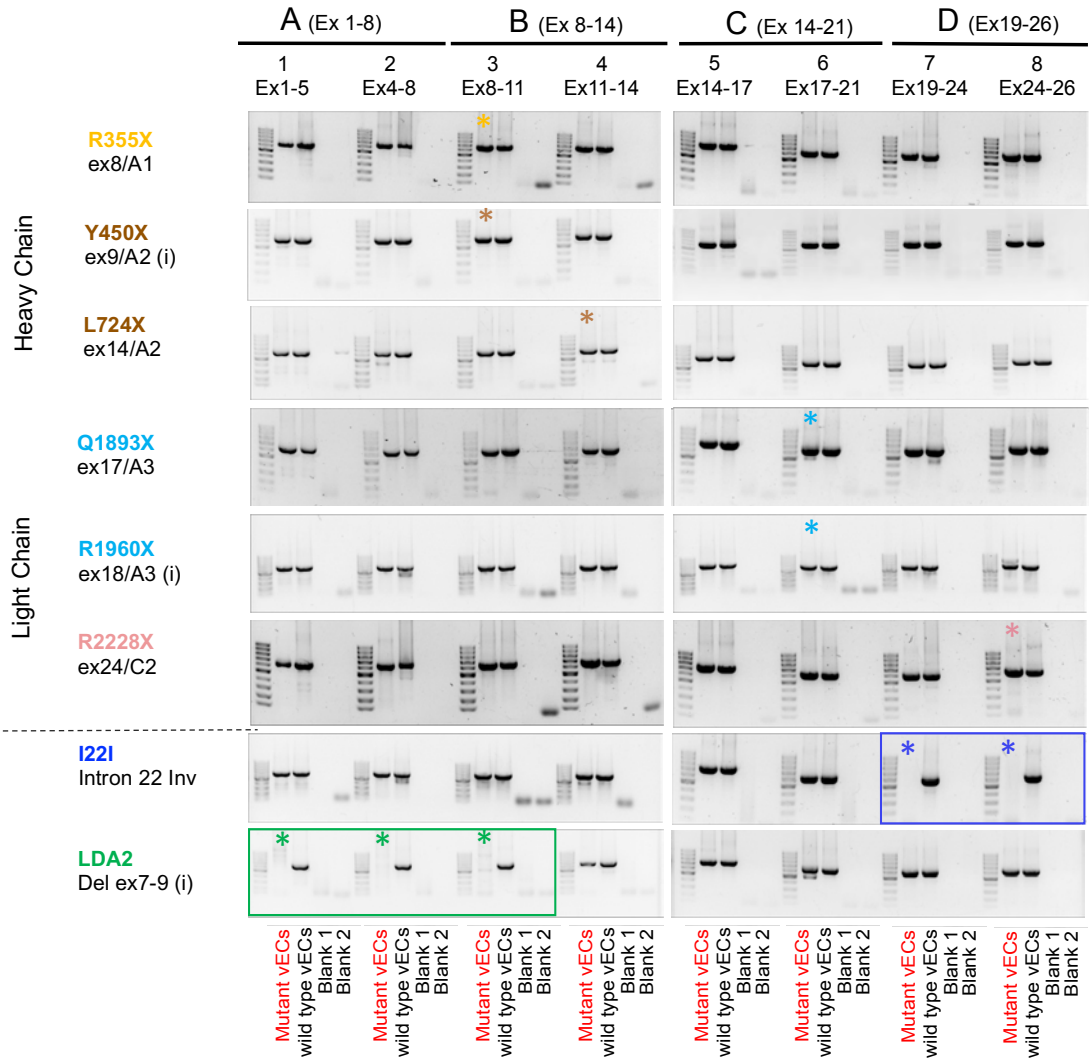

Figure S12: A. Immunostaining with anti-vWF (red) in iPS derived LEC (iLEC) , LSEC (iLSEC) iLSEC Cm1: wild type, pHDLEC: human dermal lymphatic endothelial cell, pHUVEC: human umbilical vein endothelial cell. Nuclei were counterstained with DAPi. Images were acquired using an Axio Observe 7 microscope with ApoTome.2. The objective used was a Plan-Apochromat 40x/1.4 Oil DIC M27. Images were captured with an AxioCam 702 Mono camera.

B. rt-PCR analysis of cell specific markers in vEC and iLSEC using *vWF*. LI-2D E/S: 2 days LI, 1:1 ECGM-MV2 & StemPro-34, LI-4D E/S: 4 days LI, 1:1 ECGM-MV2 & StemPro-34, LI-6D E: 6 days LI, only ECGM-MV2. E/S medium conditions consist of bFGF. Cells cultured in medium condition E does not contain bFGF, A10D: from generic vEC protocol, adding 10 days VEGF-A (Day 6-10). pHUVEC: human umbilical vein endothelial cell, pHUAEC: human umbilical arterial endothelial cell, pHDLEC: human dermal lymphatic endothelial cell, pLSEC: liver sinusoidal endothelial cell. n=200,000 cells. All data points indicate mechanical duplicates.

C. Immunostaining with biotin anti-FVIII conjugate targeting the A3 domain of FVIII visualized with Streptavidin488 (green) in primary HDLEC and anti-vWF(red). Nuclei were counterstained with DAPi. Images were acquired using an Axio Observer 7 microscope with ApoTome.2. The objective used was a Plan-Apochromat 40x/1.4 Oil DIC M27. Images were captured with an AxioCam 702 Mono camera.

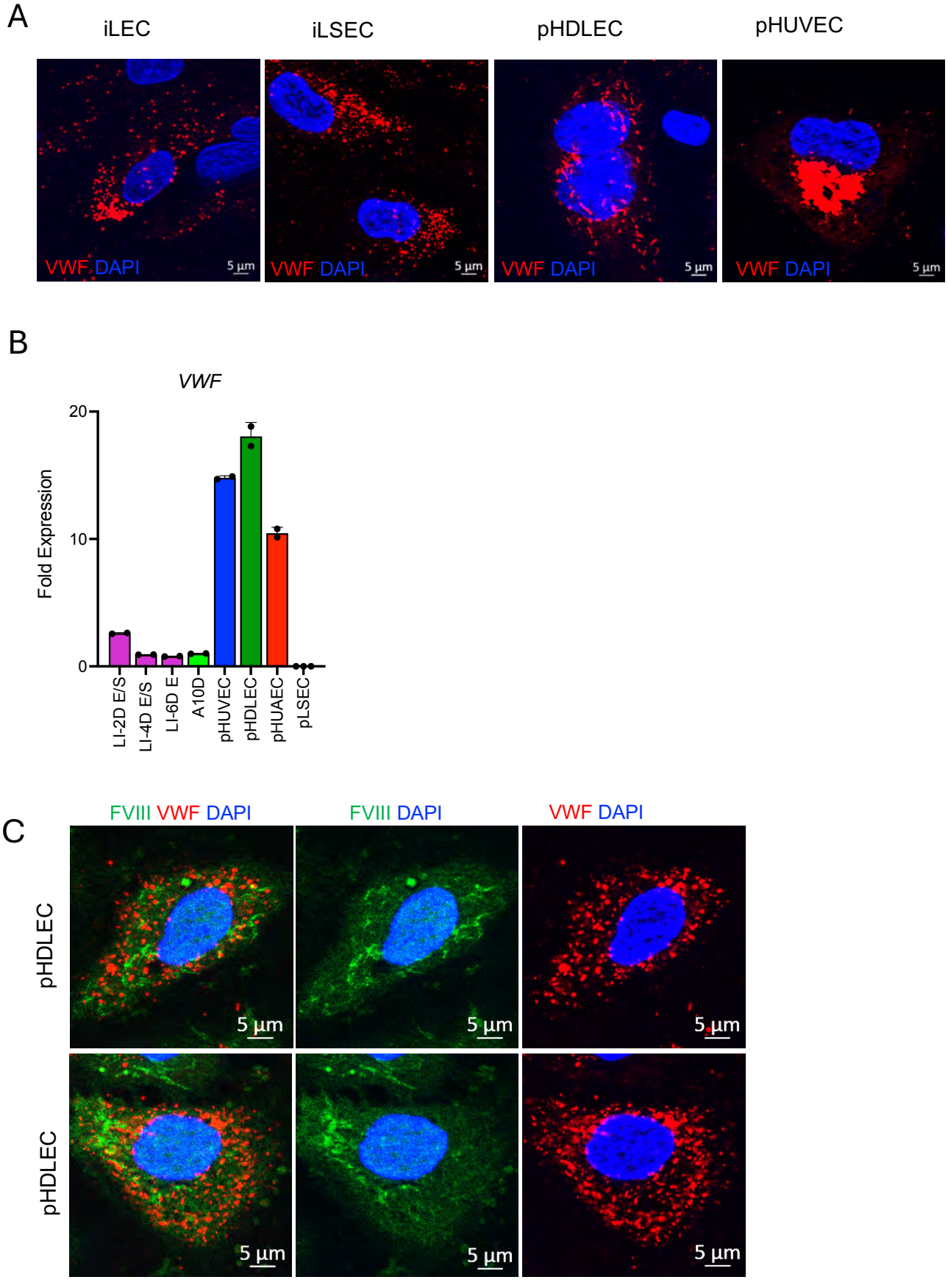
A
iLEC
iLSEC
pHDLEC
pHUVEC
VWF DAPI
5 µm
B
VWF
Fold Expression
20
10
0
LI-2D E/S
LI-4D E/S
LI-6D E
A10D
pHUVEC
pHDLEC
pHUAEC
pLSEC
C
FVIII VWF DAPI
FVIII DAPI
VWF DAPI
pHDLEC
pHDLEC
5 µm

S13: Supplementary Figure 13. MHCI peptide presentation analysis.

(A) Total number of FVIII-derived peptides identified for HLA-A, HLA-B, and HLA-C alleles.

(B) Distribution of FVIII peptides across individual HLA alleles.

(C) Predicted immunogenicity scores of peptides restricted to HLA-A, B, and C, with HLA-B showing significantly higher values. Unpaired t-test significance: ****:p<0.0001.

(D) Immunogenicity of peptides stratified by FVIII domains (A1, A2, A3, C1, C2). Representative peptide sequences, positions, domains, and scores are listed on the right. Bar graphs (far right) depict the proportion of top 10 peptides assigned to FVIII domains across the three patients (R1960X, R2228X, I22I). One-way ANOVA significance:**:p<0.01, ***:p<0.001, ****:p<0.0001.

(E) Processing score (PS) of peptides by FVIII domains. Corresponding sequences with PS values are shown on the right. Bar graphs (far right) show distribution of top 10 peptides by FVIII domains across the three patients.

(F) Predicted peptide loss associated with patient mutations. Venn diagram depicting in silico–predicted FVIII peptides absent due to the premature stop codons R1960X, R2228X, or I22I, with representative sequences.

(G) Venn diagram depicting overlap of high-immunogenic peptides among HLA-A, B, and C alleles. Shared and unique peptides are listed below.

(H) Heatmap of peptide presentation strength across HLA-A, B, and C alleles aligned to patient mutations. Right panel: Venn diagrams depicting allele-specific overlap of presented peptides across three patients.

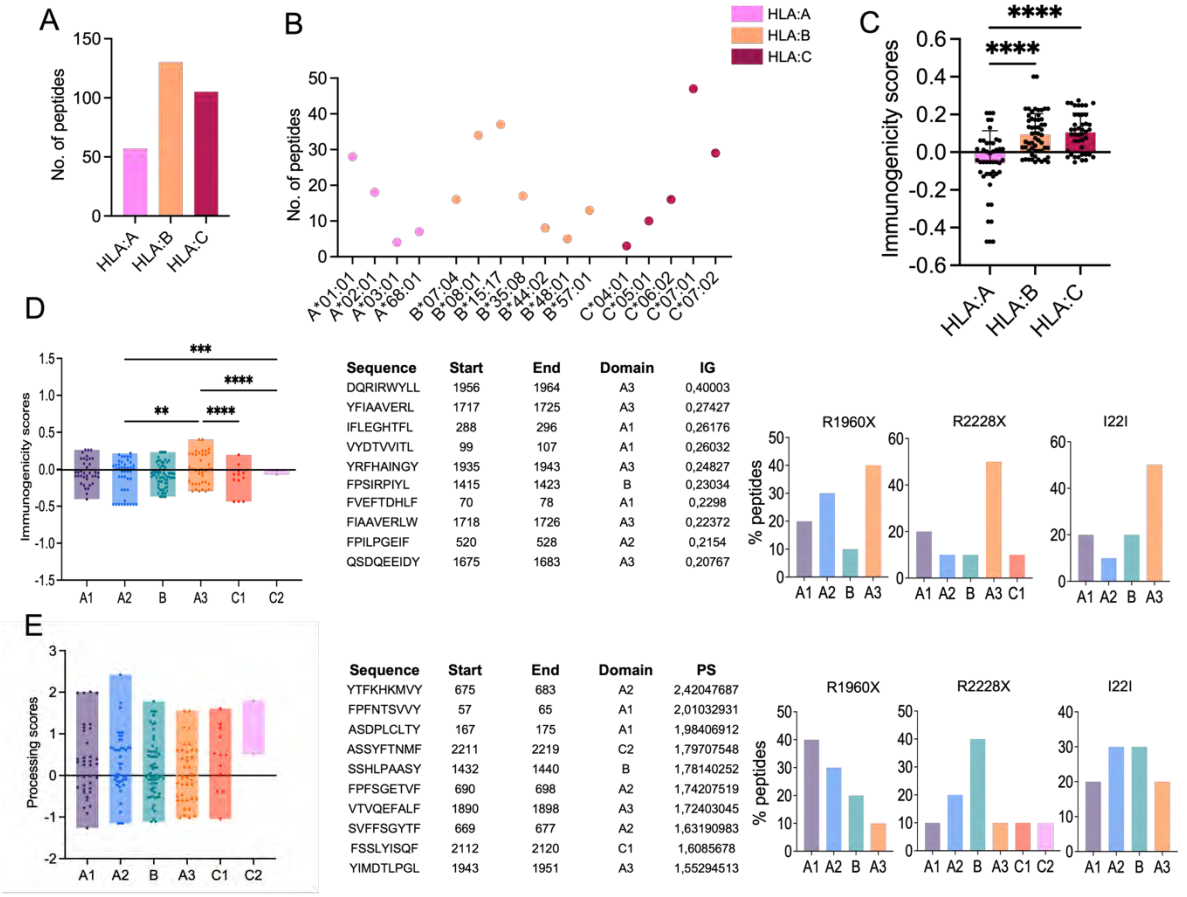
A
No. of peptides
HLA:A
HLA:B
HLA:C
B
HLA:A
HLA:B
HLA:C
No. of peptides
A*01:01
A*02:01
A*03:01
A*68:01
B*07:04
B*08:01
B*15:17
B*35:08
B*44:02
B*48:01
B*57:01
C*04:01
C*05:01
C*06:02
C*07:01
C*07:02
C
Immunogenicity scores
HLA:A
HLA:B
HLA:C
D
Immunogenicity scores
A1
A2
B
A3
C1
C2
Sequence Start End Domain IG
DQRIRWYLL 1956 1964 A3 0,40003
YFIAAVERL 1717 1725 A3 0,27427
IFLEGHTFL 288 296 A1 0,26176
VYDTVVITL 99 107 A1 0,26032
YRFHAINGY 1935 1943 A3 0,24827
FPSIRPIYL 1415 1423 B 0,23034
FVEFTDHLF 70 78 A1 0,2298
FIAAVERLW 1718 1726 A3 0,22372
FPILPGEIF 520 528 A2 0,2154
QSDQEEIDY 1675 1683 A3 0,20767
R1960X
R2228X
I22I
% peptides
E
Processing scores
Sequence Start End Domain PS
YTFKHKMVY 675 683 A2 2,42047687
FPFNTSVVY 57 65 A1 2,01032931
ASDPLCLTY 167 175 A1 1,98406912
ASSYFTNMF 2211 2219 C2 1,79707548
SSHLPAASY 1432 1440 B 1,78140252
FPFSGETVF 690 698 A2 1,74207519
VTVQEFALF 1890 1898 A3 1,72403045
SVFFSGYTF 669 677 A2 1,63190983
FSSLYISQF 2112 2120 C1 1,6085678
YIMDTLPGL 1943 1951 A3 1,55294513
R1960X
R2228X
I22I
% peptides

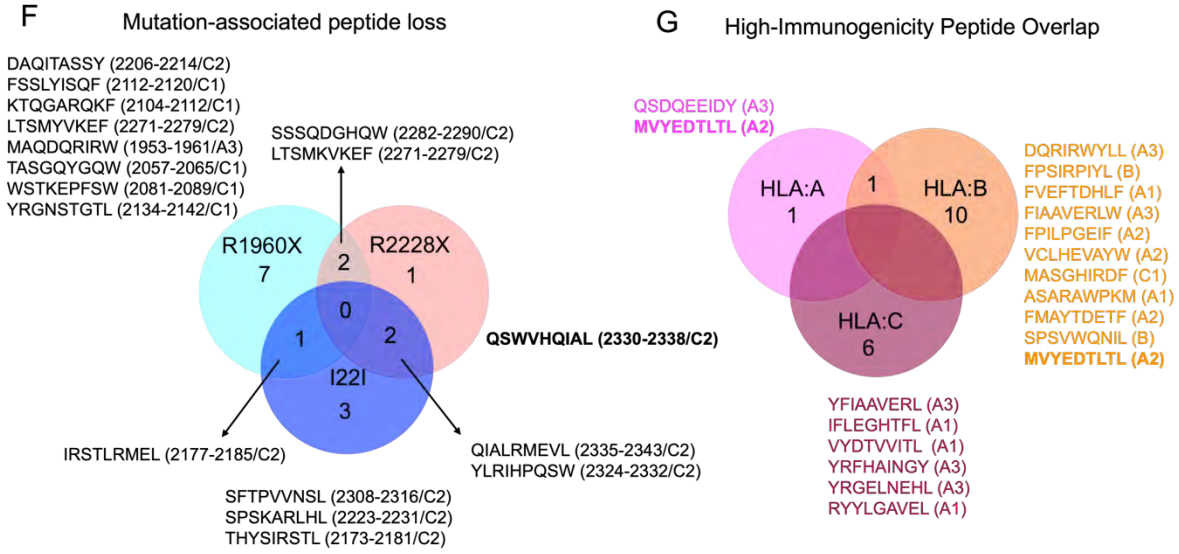
F
Mutation-associated peptide loss
DAQITASSY (2206-2214/C2)
FSSLYISQF (2112-2120/C1)
KTQGARQKF (2104-2112/C1)
LTSMYVKEF (2271-2279/C2)
MAQDQRIRW (1953-1961/A3)
TASGQYGQW (2057-2065/C1)
WSTKEPFSW (2081-2089/C1)
YRGNSTGTL (2134-2142/C1)
SSSQDGHQW (2282-2290/C2)
LTSMKVKEF (2271-2279/C2)
R1960X
7
R2228X
1
2
0
1
2
I22I
3
QSWVHQIAL (2330-2338/C2)
IRSTLRMEL (2177-2185/C2)
QIALRMEVL (2335-2343/C2)
YLRIHPQSW (2324-2332/C2)
SFTPVVNSL (2308-2316/C2)
SPSKARLHL (2223-2231/C2)
THYSIRSTL (2173-2181/C2)
G
High-Immunogenicity Peptide Overlap
QSDQEEIDY (A3)
MVYEDTLTL (A2)
HLA:A
1
1
HLA:B
10
HLA:C
6
DQRIRWYLL (A3)
FPSIRPIYL (B)
FVEFTDHLF (A1)
FIAAVERLW (A3)
FPILPGEIF (A2)
VCLHEVAYW (A2)
MASGHIRDF (C1)
ASARAWPKM (A1)
FMAYTDETF (A2)
SPSVWQNIL (B)
MVYEDTLTL (A2)
YFIAAVERL (A3)
IFLEGHTFL (A1)
VYDTVVITL (A1)
YRFHAINGY (A3)
YRGELNEHL (A3)
RYYLGAVEL (A1)

H

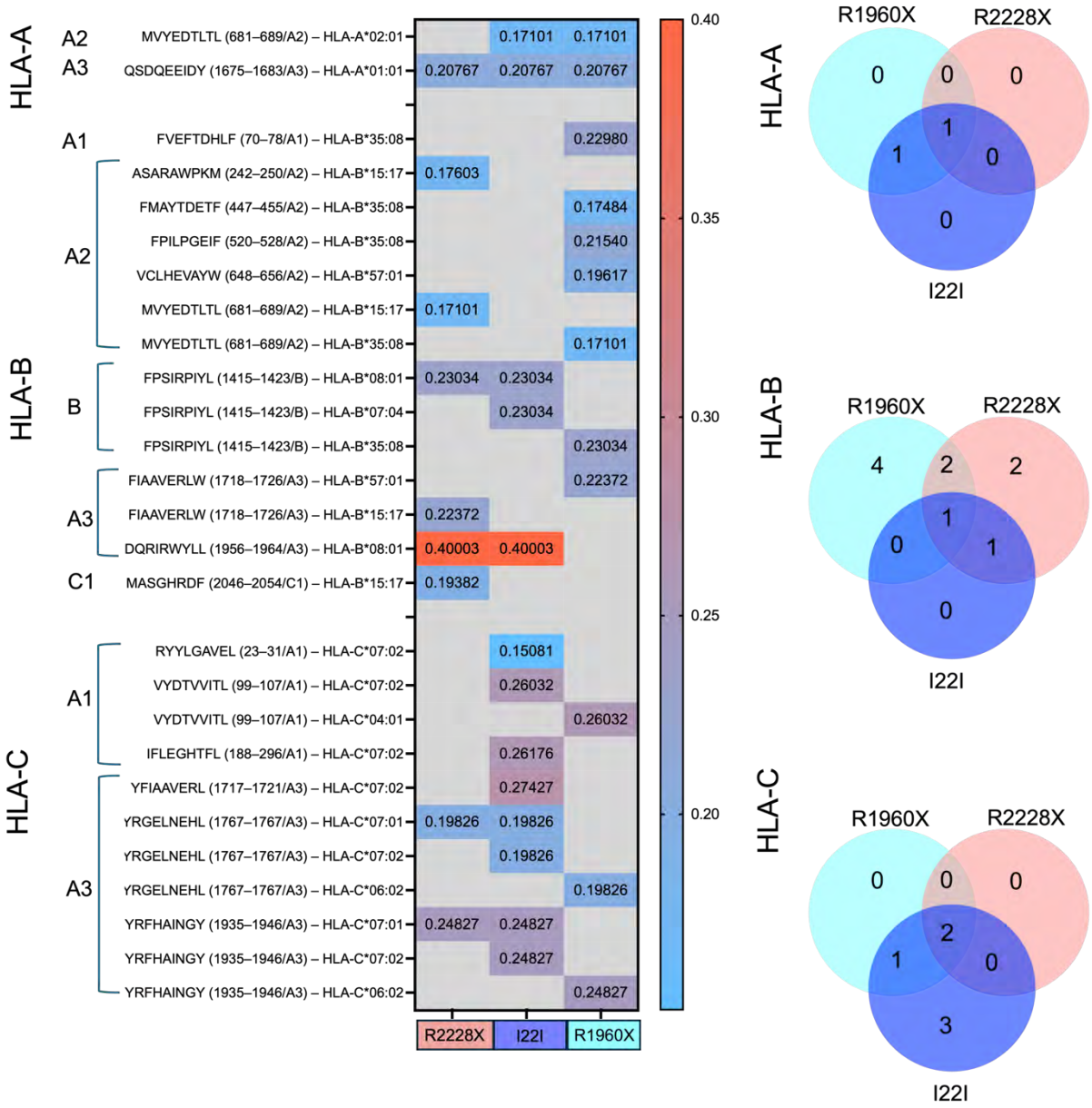
HLA-A
HLA-B
HLA-C
A2
A3
A1
A2
B
A3
C1
A1
A3
MVYEDTLTL (681–689/A2) – HLA-A*02:01
QSDQEEIDY (1675–1683/A3) – HLA-A*01:01
FVEFTDHLF (70–78/A1) – HLA-B*35:08
ASARAWPKM (242–250/A2) – HLA-B*15:17
FMAYTDETF (447–455/A2) – HLA-B*35:08
FPILPGEIF (520–528/A2) – HLA-B*35:08
VCLHEVAYW (648–656/A2) – HLA-B*57:01
MVYEDTLTL (681–689/A2) – HLA-B*15:17
MVYEDTLTL (681–689/A2) – HLA-B*35:08
FPSIRPIYL (1415–1423/B) – HLA-B*08:01
FPSIRPIYL (1415–1423/B) – HLA-B*07:04
FPSIRPIYL (1415–1423/B) – HLA-B*35:08
FIAAVERLW (1718–1726/A3) – HLA-B*57:01
FIAAVERLW (1718–1726/A3) – HLA-B*15:17
DQRIRWYLL (1956–1964/A3) – HLA-B*08:01
MASGHRDF (2046–2054/C1) – HLA-B*15:17
RYYLGAVEL (23–31/A1) – HLA-C*07:02
VYDTVVITL (99–107/A1) – HLA-C*07:02
VYDTVVITL (99–107/A1) – HLA-C*04:01
IFLEGHTFL (188–296/A1) – HLA-C*07:02
YFIAAVERL (1717–1721/A3) – HLA-C*07:02
YRGELNEHL (1767–1767/A3) – HLA-C*07:01
YRGELNEHL (1767–1767/A3) – HLA-C*07:02
YRGELNEHL (1767–1767/A3) – HLA-C*06:02
YRFHAINGY (1935–1946/A3) – HLA-C*07:01
YRFHAINGY (1935–1946/A3) – HLA-C*07:02
YRFHAINGY (1935–1946/A3) – HLA-C*06:02
0.17101 0.17101
0.20767 0.20767 0.20767
0.22980
0.17603
0.17484
0.21540
0.19617
0.17101
0.17101
0.23034 0.23034
0.23034
0.23034
0.22372
0.22372
0.40003 0.40003
0.19382
0.15081
0.26032
0.26032
0.26176
0.27427
0.19826 0.19826
0.19826
0.19826
0.24827 0.24827
0.24827
0.24827
R2228X
I22I
R1960X
0.40
0.35
0.30
0.25
0.20
HLA-A
R1960X
R2228X
0 0 0
1 0
1
0
I22I
HLA-B
R1960X
R2228X
4 2 2
1
0 1
0
I22I
HLA-C
R1960X
R2228X
0 0 0
2
1 0
3
I22I

Supplementary Figure 14. MHCII peptide presentation analysis.

(A) Total number of FVIII-derived peptides identified for HLA-DP, HLA-DQ, and HLA-DR alleles.

(B) Distribution of FVIII peptides across individual MHCII alleles.

(C) Predicted immunogenicity scores of peptides restricted to HLA-DP, DQ, and DR, with HLA-DP showing significantly higher values. Unpaired t-test significance: ***p<0.001.

(D) Immunogenicity of peptides stratified by FVIII domains (A1, A2, A3, C1). Representative peptide sequences with positions, domains, and scores are listed on the right. Bar graphs (far right) depict the proportion of top 10 peptides assigned to FVIII domains across the three patients (R1960X, R2228X, I22I). One-way ANOVA significance:*:p<0.1.

(E) Predicted cleavage probability of FVIII derived peptides by domains. Representative sequences with cleavage scores are listed on the right. Bar graphs (far right) show distribution of top 10 peptides across FVIII domains for the three patients.

(F) Predicted peptide loss associated with patient mutations. Venn diagram depicting in silico–predicted FVIII peptides absent due to the premature stop codons R1960X, R2228X, or I22I, with representative sequences listed.

(G) Venn diagram depicting overlap of high-immunogenic peptides among HLA-DP, HLA-DQ, and HLA-DR alleles. Shared and unique peptides are indicated below.

(H) Heatmaps of predicted peptide binding probability across HLA-DRB1, HLA-DRB345, HLA-DQA1/DQB1, and HLA-DPA1/DPB1 alleles aligned to patient mutations. Right panel: Venn diagrams depicting allele-specific overlap of presented peptides across three patients.

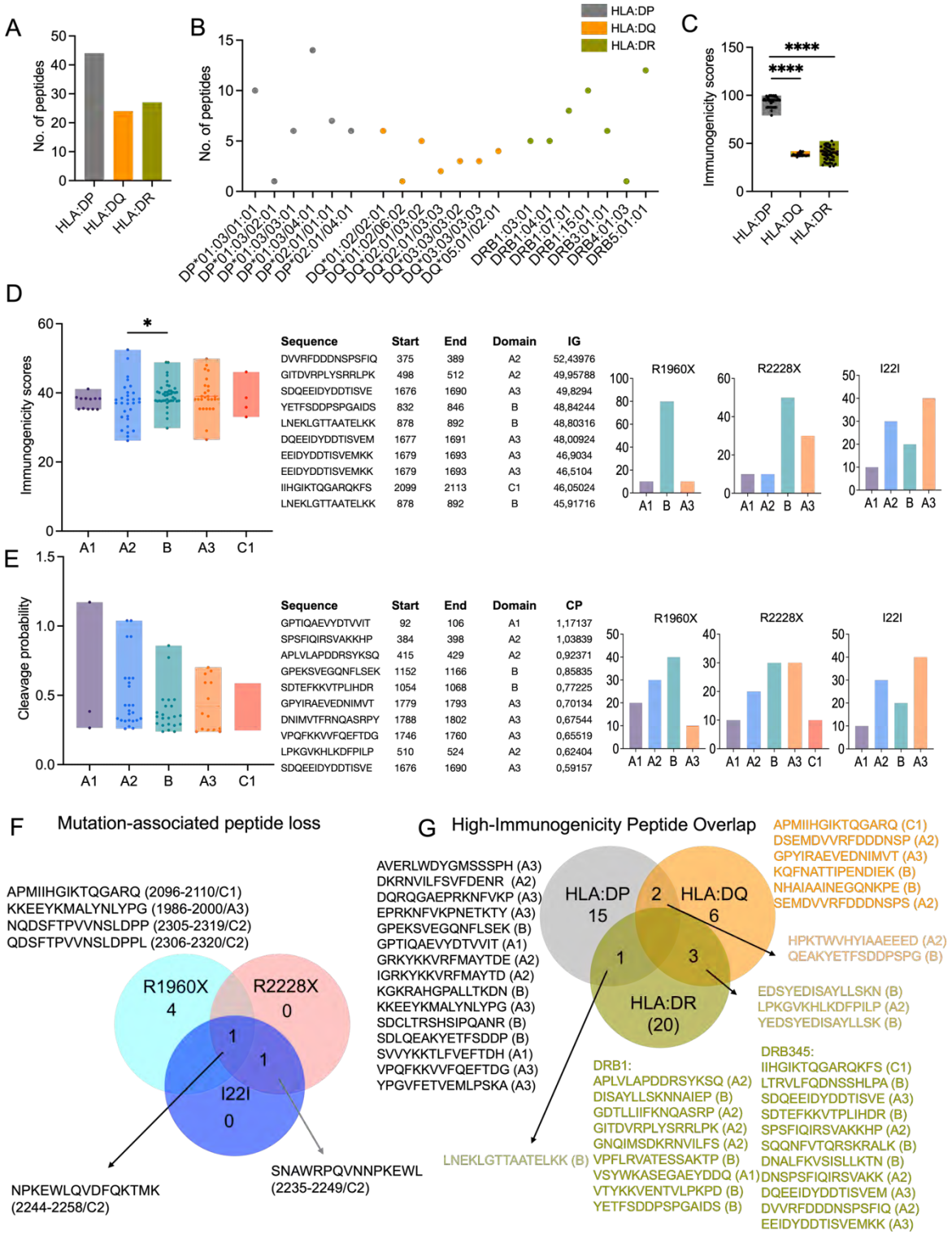
A
No. of peptides
HLA:DP
HLA:DQ
HLA:DR
B
HLA:DP
HLA:DQ
HLA:DR
No. of peptides
DP*01:03/01:01
DP*01:03/02:01
DP*01:03/03:01
DP*01:03/04:01
DP*02:01/01:01
DP*02:01/04:01
DQ*01:02/02:01
DQ*01:02/06:02
DQ*02:01/03:02
DQ*02:01/03:03
DQ*03:03/03:02
DQ*03:03/03:03
DQ*05:01/02:01
DRB1:03:01
DRB1:04:01
DRB1:07:01
DRB1:15:01
DRB3:01:01
DRB4:01:03
DRB5:01:01
C
Immunogenicity scores
****
****
HLA:DP
HLA:DQ
HLA:DR
D
Immunogenicity scores
*
A1
A2
B
A3
C1
Sequence Start End Domain IG
DVVRFDDDNSPSFIQ 375 389 A2 52,43976
GITDVRPLYSRRLPK 498 512 A2 49,95788
SDQEEIDYDDTISVE 1676 1690 A3 49,8294
YETFSDDPSPGAIDS 832 846 B 48,84244
LNEKLGTTAATELKK 878 892 B 48,80316
DQEEIDYDDTISVEM 1677 1691 A3 48,00924
EEIDYDDTISVEMKK 1679 1693 A3 46,9034
EEIDYDDTISVEMKK 1679 1693 A3 46,5104
IIHGIKTQGARQKFS 2099 2113 C1 46,05024
LNEKLGTTAATELKK 878 892 B 45,91716
R1960X
R2228X
I22I
E
Cleavage probability
A1
A2
B
A3
C1
Sequence Start End Domain CP
GPTIQAEVYDTVVIT 92 106 A1 1,17137
SPSFIQIRSVAKKHP 384 398 A2 1,03839
APLVLAPDDRSYKSQ 415 429 A2 0,92371
GPEKSVEGQNFLSEK 1152 1166 B 0,85835
SDTEFKKVTPLIHDR 1054 1068 B 0,77225
GPYIRAEVEDNIMVT 1779 1793 A3 0,70134
DNIMVTFRNQASRPY 1788 1802 A3 0,67544
VPQFKKVVFQEFTDG 1746 1760 A3 0,65519
LPKGVKHLKDFPILP 510 524 A2 0,62404
SDQEEIDYDDTISVE 1676 1690 A3 0,59157
R1960X
R2228X
I22I
F
Mutation-associated peptide loss
APMIIHGIKTQGARQ (2096-2110/C1)
KKEEYKMALYNLYPG (1986-2000/A3)
NQDSFTPVVNSLDPP (2305-2319/C2)
QDSFTPVVNSLDPPL (2306-2320/C2)
R1960X
4
R2228X
0
1
1
I22I
0
NPKEWLQVDFQKTMK
(2244-2258/C2)
SNAWRPQVNNPKEWL
(2235-2249/C2)
G
High-Immunogenicity Peptide Overlap
AVERLWDYGMSSSPH (A3)
DKRNVILFSVFDENR (A2)
DQRQGAEPRKNFVKP (A3)
EPRKNFVKPNETKTY (A3)
GPEKSVEGQNFLSEK (B)
GPTIQAEVYDTVVIT (A1)
GRKYKKVRFMAYTDE (A2)
IGRKYKKVRFMAYTD (A2)
KGKRAHGPALLTKDN (B)
KKEEYKMALYNLYPG (A3)
SDCLTRSHSIPQANR (B)
SDLQEAKYETFSDDP (B)
SVVYKKTLFVEFTDH (A1)
VPQFKKVVFQEFTDG (A3)
YPGVFETVEMLPSKA (A3)
HLA:DP
15
2
HLA:DQ
6
1
3
HLA:DR
(20)
APMIIHGIKTQGARQ (C1)
DSEMDVVRFDDDNSP (A2)
GPYIRAEVEDNIMVT (A3)
KQFNATTIPENDIEK (B)
NHAIAAINEGQNKPE (B)
SEMDVVRFDDDNSPS (A2)
HPKTWVHYIAAEEED (A2)
QEAKYETFSDDPSPG (B)
EDSYEDISAYLLSKN (B)
LPKGVKHLKDFPILP (A2)
YEDSYEDISAYLLSK (B)
DRB345:
IIHGIKTQGARQKFS (C1)
LTRVLFQDNSSHLPA (B)
SDQEEIDYDDTISVE (A3)
SDTEFKKVTPLIHDR (B)
SPSFIQIRSVAKKHP (A2)
SQQNFVTQRSKRALK (B)
DNALFKVSISLLKTN (B)
DNSPSFIQIRSVAKK (A2)
DQEEIDYDDTISVEM (A3)
DVVRFDDDNSPSFIQ (A2)
EEIDYDDTISVEMKK (A3)
DRB1:
APLVLAPDDRSYKSQ (A2)
DISAYLLSKNNAIEP (B)
GDTLLIIFKNQASRP (A2)
GITDVRPLYSRRLPK (A2)
GNQIMSDKRNVILFS (A2)
VPFLRVATESSAKTP (B)
VSYWKASEGAEYDDQ (A1)
VTYKKVENTVLPKPD (B)
YETFSDDPSPGAIDS (B)
LNEKLGTTAATELKK (B)

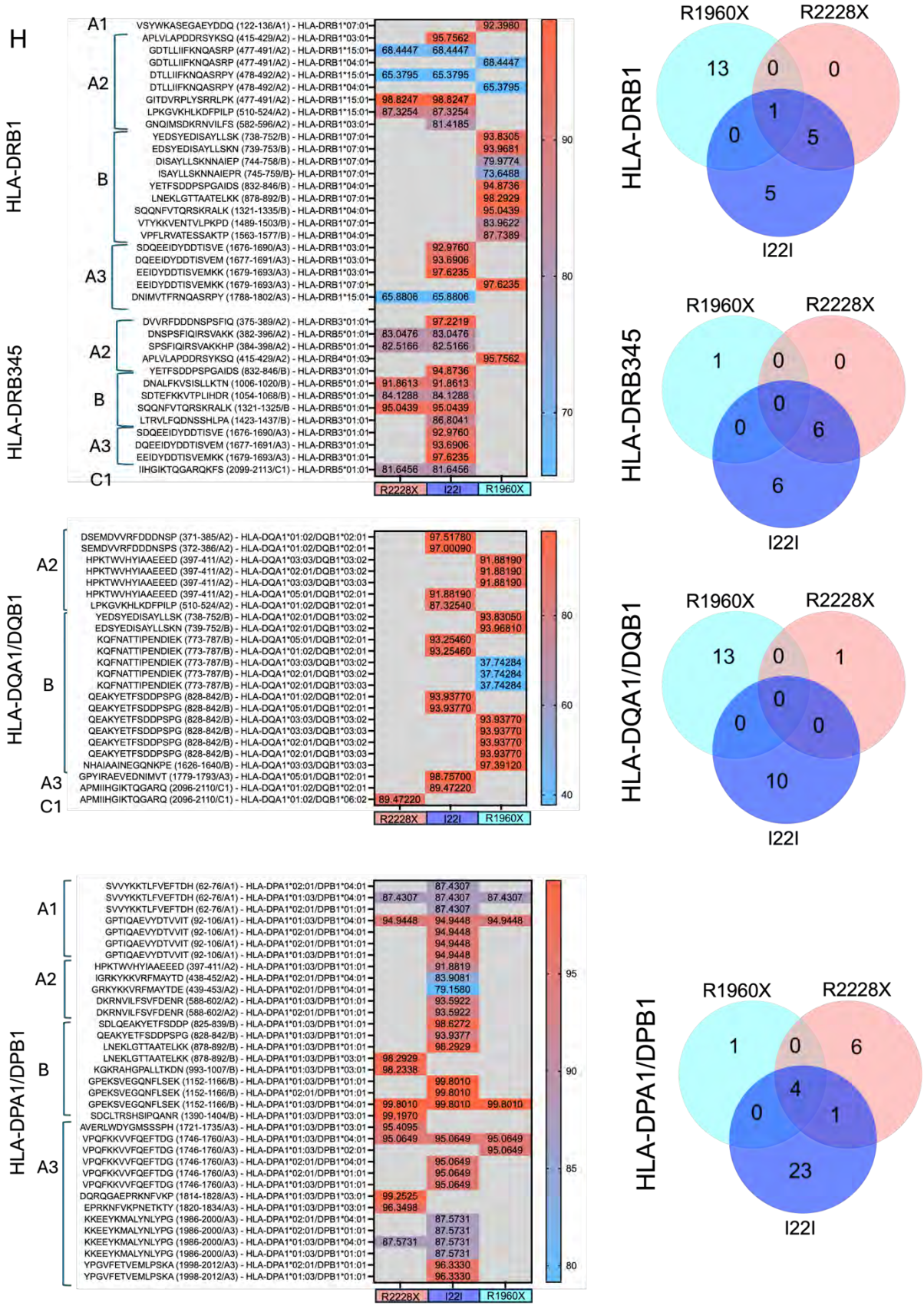
H
HLA-DRB1
HLA-DRB345
HLA-DQA1/DQB1
HLA-DPA1/DPB1
R2228X
I22I
R1960X
HLA-DRB1
HLA-DRB345
HLA-DQA1/DQB1
HLA-DPA1/DPB1

TABLE S1

REAGENT OR RESOURCE	SOURCE	IDENTIFIER
Antibodies		
Actin Smooth Muscle	ThermoFisher	Cat#MA5-11547; RRID: AB_11151920
Alpha-Fetoprotein	R&D Systems	Cat#MAB1368; RRID: AB_357658
Capture SelectTM	Thermo Fisher	Cat#7102862100
CD 144 Micro Bead Kit	Miltenyi Biotec	Cat#130-097-857;RRID: AB_2267145
CD 34 Micro Bead Kit	Miltenyi Biotec	Cat#130-046-702; RRID: AB_2848167
CD144	Santa Cruz	Cat#sc-9989; RRID: AB_2077957
CD144	BD Pharmingen	Cat#560874; RRID: AB_1645487
CD184	Miltenyi Biotec	Cat#130-117-690; RRID: AB_2728021
CD309(VEGFR2/KDR)	R&D Systems	Cat#FAB357P; RRID: AB_357165
CD31	Santa Cruz	Cat#sc-1506; RRID: AB_2161037
CD34	Miltenyi Biotec	Cat#130-113-178; RRID: AB_2726005
CD73	Miltenyi Biotec	Cat#130-123-802; RRID: AB_2889623
COPII (Sec31A)	Cell Signalling	Cat#13466; RRID: AB_2798228
GMA012	Green Mountain Antibodies	Cat#GMA012
GRP78 BiP	Abcam	Cat#ab21685; RRID: AB_2119834
LYVE1	ReliaTech	Cat#102-PA50
MHC-I PerCP-Vio700	Miltenyi Biotec	Cat#130-101-453; RRID:AB_2652093
MHC-II Clone WR18	Invitrogen	Cat#MA180680; RRID: AB_931650
Nanog	PeproTech	Cat#500-P236; RRID: AB_2929970
Oct4	abcam	Cat#ab19857; RRID: AB_445175
PDI (C81H6)	Cell Signalling	Cat#3501; RRID: AB_2156433
PROX-1	Abcam	Cat#ab101851; RRID: AB_10712211
SAF8C (affinity purified)	Affinity Biologicals	Cat#SAF8C-AP
SAF8C Peroxidase conjugated	Coachrom Diagnostica	Cat#SAF8C-HRP
SEL1L	antibodies-online	Cat#ABIN6132642
SSEA-4	Stemcell Technologies	Cat#60062; RRID: AB_2721031
ß-Tubulin	Stemcell Technologies	Cat#60100
STAB2	Abcam	Cat#ab121893; RRID: AB_11132688
Streptavidin Alexa 488	ThermoFisher	Cat#S32354; RRID: AB_2315383
Tra-1-60	Millipore	Cat#MAB4360; RRID: AB_2119183
VE-Cadherin	Santa Cruz	Cat#sc-9989; RRID: AB_2077957
vWF	Dako	Cat#A0082; RRID: AB_2315602
Chemicals, peptides, and recombinant proteins		
8-Br-cAMP	Biolog Life Science institute	BLG-B007-500
Accutase	Capricorn	ACC-1B
B27+Vit A	Thermofischer Scientific	17504-044
bFGF	PeproTech	100-18C-100
BMP4	PeproTech	120-05ET-10
BSA	Sigma	A1595
CHIR 99021	Biogems	2520691

DMEM F12/Glutamax	Thermofischer Scientific	31331093
ECGM-MV2	PromoCell	22121
EDTA	Sigma	E5134
ELISA substrate	Sigma Aldrich	11582950001
Fibronectin	Roche	10838039001
Forskolin	Stemcell	72114
Glycine	Geyer GmbH & Co. KG	3790.2
Growth factor reduced Matrigel	Corning	356230
IFN-γ	PeproTech	300-02-100
IL-1β	PeproTech	200-01B-10
IL-3	PeproTech	200-03-10
IL-6	PeproTech	200-06-20
L-685 458	Sigma	L1790
LDL-DyLightTM 550	Abcam	ab133127
Matrigel hESC-Quali mouse	Corning	354277
mTesR complete kit	Stemcell	85850
N2	Thermofischer Scientific	17502-048
NP40	Sigma Aldrich	R0278
Parafolmaldehyde	Sigma Aldrich	P6148
Penicillin-Streptomycin	Thermofischer Scientific	15070063
Protease inhibitor	Roche	4693159001
PureLink RNA Mini Kit	Invitrogen	12183018A
Purified Streptavidin	BioLegend	280302
ReadyProbesTM Streptavidi/Biotin blocking solution	ThermoFisher	R37628
Saponin	Fisher Scientific	15460297
SB-431542	BioVision	AOB 6359-1
Stempro 34 Kit	Thermofischer Scientific	10639011
TNF-α	PeproTech	300-01A-50
VEGF-A	PeproTech	100-20
VEGF-C	PeproTech	100-20-CD-100
Y-27632	Stemcell	2304
Critical commercial assays		
AgPath-ID-One step-RT-PCR Kit	Applied Biosystems	4387424
CaptureM™ IP & Co-IP kit	Takara	635721
Experimental models: Cell lines		
pHDLEC	Promocell	C-14021
pHUAEC	Promocell	C-14013
pHCMEC	Promocell	C-14029
pHUVEC	Promocell	C-14010
pLSEC	Neuromics	HEC11
Oligonucleotides and Primers		
AY-Actin F	Eurofins Genomics	ACC TTC TAC AAT GAG CTG CG
AY-Actin R	Eurofins Genomics	CCT GGA TAG CAA CGT ACA TGG
Probe-ACT	Eurofins Genomics	ACC TGG GTC ATC TTC TCG CGG TTG
PROX-1-F	Eurofins Genomics	GCC AGA TTT GCA GTC AAT GG
PROX-1-R	Eurofins Genomics	ATG ATG ACG TCG CCA AAG C
PROX-1-FAM	Eurofins Genomics	TTT CCA CAC CGC CAA C
PDPN-F	Eurofins Genomics	CAG GTG CCG AAG ATG ATG TG
PDPN-R	Eurofins Genomics	TGT TGC CAC CAG AGT TGT CA
PDPN-FAM	Eurofins Genomics	TGA CTC CAG GAA CCA G
LYVE-1 F	Eurofins Genomics	CTG GGT TGG AGA TGG ATT CG
LYVE-1 R	Eurofins Genomics	TCA GGA CAC CCA CCC CAT TT
LYVE1-FAM	Eurofins Genomics	TAG CCC AAA CCC CAA GTG

VEGFR3-F	Eurofins Genomics	CCT TGC CCG GGA CAT CTA
VEGFR3-R	Eurofins Genomics	TTG TCG AAG ATG CTT TCA GGG
VEGFR3-FAM	Eurofins Genomics	AGA CCC CGA CTA CGT CCG CAA GG
STAB2	Thermofischer Scientific	Hs00213948_m1
FCGR2B	Thermofischer Scientific	Hs00269610_m1
F8	Thermofischer Scientific	Hs00252034_m1
COUP-TFII	Thermofischer Scientific	Hs00819360_m1 I
VEGFR2	Thermofischer Scientific	Hs00911700_m1
NT5E	Thermofischer Scientific	Hs0015968_m1
Eph-B2	Thermofischer Scientific	Hs00187950_m1
vWF Ex38-39	Thermofischer Scientific	Hs01109449_m1
CD31	Thermofischer Scientific	Hs01065279_m1
CD34	Thermofischer Scientific	Hs02576480_m1
CD144 Ex3-4	Thermofischer Scientific	Hs00901465_m1
NANOG	Thermofischer Scientific	Hs02387400_g1
SOX2	Thermofischer Scientific	Hs04234836_s1
Brachyury	Thermofischer Scientific	Hs00610080_m1
Software and algorithms		
FlowJo	Tree Star	Version 10.9
GraphPad Prism	GraphPad Software	Version 10.4.1
Others		
0.45 µM filter	Berrytec	110597
LS columns	Miltenyi Biotec	130-042-401
MaxiSorp C8x12 (ELISA Plates)	VWR	735-0006
MicroAmp Optical 8-Cap Strip	Applied Biosystems	4323032
MicroAmp Optical 8-tube Strip (0.2mL)	Applied Biosystems	4316567
Vivaspin 6, MWCO: 50K	Sartorius	ST-2638
Mini Protean 7.5% MP TGX Gel	Biorad	4561024

Table S2: Quantitation for FVIII peptides detected in healthy. Green: High confidence peptides. M: measurement.

Peptide	First Position	Last Position	Healthy M1 Total area	Healthy M2 Total area
PYNIYPHGITDVRPLYSR	491	508		
DFPILPGEIFK	519	529	8,8E+05	
NVILFSVFDENR	591	602	4,5E+05	
SVEGQNFLSEK	1156	1166		
LWDYGMSSSPHVLR	1725	1738		
GELNEHLGLLGPYIR	1769	1783		2,0E+06
VDLLAPMIIHGIK	2092	2104		2,2E+05
HNIFNPPIIAR	2156	2166		
SNAWRPQVNNPK	2235	2246		1,7E+05
IHPQSWVHQIALR	2327	2339	7,0E+05	

Table S3: Quantification for Protein Disulfide Isomerase (PDI), an endoplasmic reticulum (ER) marker, and COPII as a marker for the ER-Golgi intermediate compartment (ERGIC) to localize FVIII in iLSEC

FVIII & PDI																						
Number of families	1																					
Number of comparisons per family	3																					
Alpha	0,05																					
																	Cm1	I22I	R1960X	R2228X		
Dunnett's multiple comparisons test	Mean Diff.	95,00% CI of diff.	Below threshold?	Summary	Adjusted P	A-?									Number of values		59	65	65	57	65	
Cm1 vs. I22I	0,2195	0,1481 to 0,2908	Yes	****	<0,0001	B	I22I															
Cm1 vs. R1960X	0,07226	-0,001458 to 0,1460	No	ns	0,0561	C	R1960X								Minimum		0,2896	0,2086	0,1129	0,1885		
Cm1 vs. R2228X	0,05809	-0,01329 to 0,1295	No	ns	0,1376	D	R2228X								Maximum		0,925	0,8235	0,8717	0,8779		
															Range		0,6354	0,615	0,7589	0,6894		
Test details	Mean 1	Mean 2	Mean Diff.	SE of diff.	n1	n2		q	DF													
Cm1 vs. I22I	0,6617	0,4422	0,2195	0,03022	59		65	7,261	242						Mean		0,6617	0,4422	0,5894	0,6036		
Cm1 vs. R1960X	0,6617	0,5894	0,07226	0,03122	59		57	2,315	242						Std. Deviation		0,1503	0,1628	0,1932	0,1649		
Cm1 vs. R2228X	0,6617	0,6036	0,05809	0,03022	59		65	1,922	242						Std. Error of Mean		0,01957	0,02019	0,02559	0,02045		
FVIII & BiP																						
Number of families	1																					
Number of comparisons per family	3																					
Alpha	0,05																					
																	Cm1	I22I	R1960X	R2228X		
Dunnett's multiple comparisons test	Mean Diff.	95,00% CI of diff.	Below threshold?	Summary	Adjusted P	A-?									Number of values		45	57	38	61		
Cm1 vs. I22I	0,2882	0,1892 to 0,3872	Yes	****	<0,0001	B	I22I															
Cm1 vs. R1960X	0,0421	-0,06727 to 0,1515	No	ns	0,6814	C	R1960X								Minimum		0,05804	0,00255	0,05121	0,03188		
Cm1 vs. R2228X	0,1884	0,09080 to 0,2859	Yes	****	<0,0001	D	R2228X								Maximum		0,8657	0,6929	0,9326	0,7666		
															Range		0,8076	0,6904	0,8814	0,7348		
Test details	Mean 1	Mean 2	Mean Diff.	SE of diff.	n1	n2		q	DF													
Cm1 vs. I22I	0,5545	0,2663	0,2882	0,04192	45		57	6,875	197						Mean		0,5545	0,2663	0,5124	0,3661		
Cm1 vs. R1960X	0,5545	0,5124	0,0421	0,04631	45		38	0,9091	197						Std. Deviation		0,2576	0,1906	0,2237	0,178		
Cm1 vs. R2228X	0,5545	0,3661	0,1884	0,04131	45		61	4,56	197						Std. Error of Mean		0,03839	0,02524	0,03629	0,02279		
FVIII & SEL1L																						
Number of families	1																					
Number of comparisons per family	3																					
Alpha	0,05																					
																	Cm1	I22I	R1960X	R2228X		
Dunnett's multiple comparisons test	Mean Diff.	95,00% CI of diff.	Below threshold?	Summary	Adjusted P	A-?									Number of values		31	37	52	35		
Cm1 vs. I22I	0,05615	-0,05548 to 0,1678	No	ns	0,48	B	I22I															
Cm1 vs. R1960X	-0,1093	-0,2133 to -0,005241	Yes	*	0,0371	C	R1960X								Minimum		0,01433	0,00493	0,00526	0,00917		
Cm1 vs. R2228X	-0,04814	-0,1612 to 0,06493	No	ns	0,6047	D	R2228X								Maximum		0,6443	0,6967	0,8005	0,6979		
															Range		0,6299	0,6917	0,7952	0,6888		
Test details	Mean 1	Mean 2	Mean Diff.	SE of diff.	n1	n2		q	DF													
Cm1 vs. I22I	0,2719	0,2157	0,05615	0,04732	31		37	1,187	151						Mean		0,2719	0,2157	0,3812	0,32		
Cm1 vs. R1960X	0,2719	0,3812	-0,1093	0,0441	31		52	2,478	151						Std. Deviation		0,1791	0,1638	0,2186	0,1983		
Cm1 vs. R2228X	0,2719	0,32	-0,04814	0,04793	31		35	1,004	151						Std. Error of Mean		0,03217	0,02693	0,03032	0,03351		

Table S4: HLA genotypes of the three analyzed HA patients (R2228X, R1960X with inhibitor, and I22I) including class I (HLA-A, B, C) and class II (HLA-DR, DQ, DP) alleles.

	R2228X:	R1960X (Inhibitor):	I22I:
DRB1	HLA-DRB1*15:01	HLA-DRB1*04:01 HLA-DRB1*07:01	HLA-DRB1*03:01 HLA-DRB1*15:01
DRB345	HLA-DRB5*01:01	HLA-DRB4*01:03	HLA-DRB3*01:01 HLA-DRB5*01:01
DQA1/DQB1	HLA-DQA1*01:02/DQB1*06:02	HLA-DQA1*02:01/DQB1*03:03 HLA-DQA1*02:01/DQB1*03:02 HLA-DQA1*03:03/DQB1*03:03 HLA-DQA1*03:03/DQB1*03:02	HLA-DQA1*01:02/DQB1*02:01 HLA-DQA1*05:01/DQB1*02:01
DPA1/DPB1	HLA-DPA1*01:03/DPB1*03:01 HLA-DPA1*01:03/DPB1*04:01	HLA-DPA1*01:03/DPB1*02:01 HLA-DPA1*01:03/DPB1*04:01	HLA-DPA1*01:03/DPB1*01:01 HLA-DPA1*01:03/DPB1*04:01 HLA-DPA1*02:01/DPB1*01:01 HLA-DPA1*02:01/DPB1*04:01

	R2228X:	R1960X (Inhibitor):	I22I:
HLA-A	HLA-A*01:01 HLA-A*68:01	HLA-A*01:01 HLA-A*02:01	HLA-A*01:01 HLA-A*02:01
HLA-B	HLA-B*15:17 HLA-B*08:01	HLA-B*35:08 HLA-B*57:01	HLA-B*07:04 HLA-B*08:01
HLA-C	HLA-C*07:01	HLA-C*04:01 HLA-C*06:02	HLA-C*07:01 HLA-C*07:02